Hybrid semi-batch/batch reverse osmosis (HSBRO) for use in zero liquid discharge (ZLD) applications

Hosseinipour, Ebrahim; Karimi, Somayeh; Barbe, Stéphan; Park, Kiho; Davies, Philip A.

DOI:
10.1016/j.desal.2022.116126

Document Version
Publisher's PDF, also known as Version of record

Citation for published version (Harvard):
Hosseinipour, E, Karimi, S, Barbe, S, Park, K & Davies, PA 2022, 'Hybrid semi-batch/batch reverse osmosis (HSBRO) for use in zero liquid discharge (ZLD) applications', *Desalination*, vol. 544, 116126. https://doi.org/10.1016/j.desal.2022.116126

Desalination 544 (2022) 116126

Contents lists available at ScienceDirect

Desalination

journal homepage: www.elsevier.com/locate/desal

Hybrid semi-batch/batch reverse osmosis (HSBRO) for use in zero liquid discharge (ZLD) applications

Ebrahim Hosseinipour [a], Somayeh Karimi [a], Stéphan Barbe [b], Kiho Park [c], Philip A. Davies [a,*]

[a] School of Engineering, University of Birmingham, Edgbaston, Birmingham B15 2TT, United Kingdom of Great Britain and Northern Ireland
[b] Faculty of Applied Natural Sciences, Technische Hochschule Köln, Kaiser-Wilhelm-Allee, Gebäude E39, 51373 Leverkusen, Germany
[c] School of Chemical Engineering, Chonnam National University, 77 Yongbong-ro, Buk-gu, Gwangju 61186, Republic of Korea

HIGHLIGHTS

- HSBRO is more efficient than semi-batch RO and more compact than batch RO.
- Specific energy consumption of 0.54 kWh/m^3 at recovery of 0.94 with 1.5 g/L feed salinity
- Model agrees with experiments within 3 % error.
- 2nd law efficiency of 7.8–17.8 % obtained, with 22.8–34.5 % predicted after technical improvements
- Feed of salinity up to 6 g/L may be treated with recovery of 0.95 and system pressure < 120 bar.

GRAPHICAL ABSTRACT

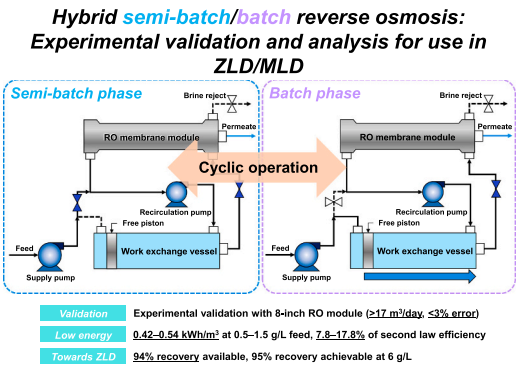

ARTICLE INFO

Keywords:
High recovery
Energy efficiency
Batch reverse osmosis
Salt retention
Zero liquid discharge

ABSTRACT

Hybrid semi-batch/batch reverse osmosis (HSBRO) is a new method of high-recovery desalination that provides low Specific Energy Consumption (*SEC*) in a compact design. In this first experimental study on HSBRO, we report *SEC* over a range of operating parameters using brackish feed water. For example, at 500–1500 mg/L feed concentration, and recovery of 0.94, we measured hydraulic and electrical *SEC* of 0.20–0.31 kWh/m^3 and 0.42–0.54 kWh/m^3 respectively, using a flux of 18.9 L/m^2/h and obtaining an output of 17.5 m^3/day. Second law efficiency was 7.8–17.8 % thus improving on available multistage and semi-batch RO systems. A model of the system, that includes the effect of finite salt rejection, predicts *SEC* with accuracy of 1–3 %. With improvements in membrane permeability, valves, and pump efficiency, we predict electrical *SEC* lowered to 0.14–0.28 kWh/m^3 and second law efficiency elevated to 22.8–34.5 %. Though simple batch RO can achieve comparable *SEC* to HSBRO, for recovery as high as 0.94 it would require an impractically large work exchanger. The model shows that feed of salinity up to 6000 mg/L may be treated with recovery of 0.95 and peak system pressure < 120 bar, indicating great potential in ZLD and MLD applications.

* Corresponding author.
E-mail address: p.a.davies@bham.ac.uk (P.A. Davies).

https://doi.org/10.1016/j.desal.2022.116126
Received 18 May 2022; Received in revised form 15 September 2022; Accepted 18 September 2022
Available online 30 September 2022

1. Introduction

The worldwide demand for new sources of water has increased in recent decades because of rapid population growth, climate change, increased per capita domestic usage, and increased industrial and agricultural water requirements [1–4]. Desalination is being increasingly adopted to address this problem. The two most common approaches to desalination are thermal- and membrane-based technologies. Thermal technologies are highly energy-intensive, requiring many times the theoretical minimum energy of separation. In contrast, membrane technologies are becoming more popular due to their greater energy efficiency, reduced equipment size, and more flexible capacity [3,5–9].

Reverse osmosis (RO), the most common membrane desalination technology, currently dominates the desalination industry [10–12]. But despite its benefits, RO also has drawbacks. First, like other desalination technologies, RO plants discharge highly saline brine and chemicals which pose a risk to the environment [11]. Second, the energy consumption of RO systems is still higher than the theoretical minimum and efforts to reduce energy consumption are therefore ongoing.

To address the first drawback, the zero liquid discharge (ZLD) approach has been proposed. As the growing concerns about waste disposal increase, ZLD is becoming more important to eliminate liquid waste and maximize water recovery [13]. ZLD is attracting significant interest in recent years in sustainable desalination and wastewater treatment, to overcome waste disposal hazards and concerns [10,14,15]. In particular, ZLD has a crucial role in the desalination of brackish groundwater, where high recovery of water and elimination of brine discharge is needed in inland agricultural and municipal applications [16,17]. However, ZLD processes tend to be energy-intensive since they attempt to separate all impurities from the effluent stream [13,14]. Therefore, minimal liquid discharge (MLD) has also been put forward as an approach to minimize (though not completely eliminate) brine discharge, while incurring lower energy consumption than ZLD [18].

ZLD and MLD schemes use either membrane or non-membrane technologies. Non-membrane technologies include mechanical/thermal evaporation methods such as MVC (mechanical vapour compression). This traditional technique is highly energy-intensive with a reported *SEC* of 20–40 kWh/m^3 [14,19–21]. Such methods have mostly been used for feeds with high salinities such as concentrated brines and seawater. Among the membrane-based methods, including electrodialysis and membrane distillation, RO is an energy-efficient and cost-effective method with energy consumption as low as 2–4 kWh/m^3 with seawater [20]. However, the application of RO in ZLD/MLD systems is limited by membrane burst pressure and fouling at high salinity. Therefore, RO has mostly been used as the initial concentration step before a thermal process to achieve ZLD/MLD [22]. High recovery RO, with its superior energy efficiency, would offer great promise in ZLD/MLD by helping to reduce the size of downstream thermal treatment units [13]. Recently, new RO technologies such as osmotically-assisted reverse osmosis (OARO) [19,23–27], high pressure reverse osmosis (HPRO) [28], low-salt-rejection reverse osmosis (LSRRO) [18,19], and cascading osmotically mediated RO (COMRO) [19,29,30] were shown to be technically and economically favourable in high-recovery applications for ZLD and MLD. However, only a few experimental works have been reported using such methods [30–33].

In response to the second drawback of RO, over the last few decades a number of approaches have helped to improve energy efficiency, including energy recovery devices (ERDs), more efficient pumps, osmotic pre-dilution to reduce feed salinity, the use of technologies to recover osmotic energy in the form of pressure-retarded osmosis (PRO) or reverse electrodialysis (RED), multi-stage RO, and novel RO configurations [3,5,15]. Nevertheless, the RO process still requires further research to reduce the energy consumption [3]. To this end, several innovative concepts have been proposed. For example, energy-efficient reverse osmosis (EERO) has been developed to overcome the problem of excessively high pressure in RO when targeting increased water recovery [34–39]. Centrifugal RO (CRO) was also proposed to reduce energy consumption relative to single-stage RO [40]. Moreover, several configurations of staged RO, batch RO and semi-batch RO (or closed-circuit desalination) have been proposed to enhance the energy efficiency of RO as well as enhancing water recovery. Some proposals were based on modelling [8,9,13,15,41–50]; and others on experimental studies [17,41,44,45,47,50–56]. Table 1 summarizes the experimental performance of some RO-based treatment technologies with high recovery (>0.7) which can be considered for use in ZLD and MLD applications.

Several researchers have carried out comparisons among different configurations of RO in terms of performance and energy consumption [9,13,42,49]. At recovery up to about 0.7, semi-batch RO offers comparable energy consumption to three-stage RO but in a more practical, compact and economical configuration [42,49]. However, batch RO is an even more promising method for improving the energy efficiency of RO systems when high recovery is needed [15].

Using batch RO technology, desalination can be achieved with minimal energy consumption, even at high recoveries [46]. For example, Davies et al. [47] constructed a batch RO prototype and achieved a hydraulic *SEC* of 0.31 kWh/m^3 and recovery of 0.69 with feedwater salinity of 5000 mg/L. Park et al. [46] modelled the design and operation of a single-acting batch RO system that operates cyclically in two phases, using a work exchanger to transfer pressure from the feed fluid to the recirculating side. Their batch RO model showed promising results including water recovery of 0.8 and low energy consumption with second law efficiency of 33.2 %. Recently, Hosseinipour et al. [44] presented an extensive experimental study of a batch RO system for brackish water treatment and modified the model in [46] by including the osmotic backflow effect. The experiments showed a recovery of 0.8, hydraulic *SEC* in the range 0.22–0.48 kWh/m^3 and electrical *SEC* in the range 0.48–0.83 kWh/m^3. Cordoba et al. [48] modelled a double-acting batch RO configuration that used a high-pressure tank with a reciprocating piston. The study calculated a specific energy consumption of 1.88 kWh/m^3 for seawater with a salinity of 35,000 mg/L, recovery of 0.5, and a permeate flux of 15 L/m^2/h. Wei et al. [50] experimentally studied a batch RO system using a flexible bladder as the work exchanger, and predicted a 11 % energy saving compared to a single-stage RO for seawater at recovery of 0.5.

Although batch RO is an excellent candidate for high-recovery and energy-efficient desalination, the system size increases sharply as recovery increases above about 0.7, because of the large volume required of the work exchanger vessel. To overcome this practical drawback, Park et al. [15] introduced a hybrid semi-batch/batch reverse osmosis (HSBRO) concept as a high-recovery, compact, and energy-efficient system. This hybrid design was predicted to approach the energy efficiency of batch RO in a more compact format. With the proposed novel design of HSBRO, the volume of work exchanger vessel is several times smaller than in batch RO at the recovery of 0.95, whereas only a small energy penalty (<5 %) is incurred compared to batch RO.

However, this hybrid concept has yet to be validated experimentally [15]. Therefore, the main objective of the present study is to investigate the HSBRO system at pilot scale and evaluate its performance in treating brackish feed water. A series of experiments has been performed at several feed salinities and water permeate fluxes. The system performance is studied including hydraulic and electrical *SEC*, salt retention effect, permeate and batch conductivity, concentration factor and recovery. Moreover, the model developed by Park et al. [15] has been modified and adjusted in light of the experimental findings. This study further aims to use the validated mathematical model to predict the HSBRO system performance in applications at higher salinities and pressures. Although the RO system of this study is limited to 25 bar, the experiments validate the HSBRO concept as a preconcentration stage for ZLD/MLD that will be applicable for a higher range of pressures and concentrations. For example, besides treating brackish water, the concept may in the future be applied to the concentration of metal

Table 1
Comparison of experimental performances of RO-based technologies operating at high recovery. In general, the *SEC* values are electrical energy per m^3 of output. However, refs. [57] and [58] do not distinguish between hydraulic and electrical *SEC*; ref. [58] gives *SEC* per m^3 of input.

Technology	Feed TDS (mg/L)	Recovery (%)	*SEC* (kWh/m^3)	System output (m^3/day)	Reference
Batch RO	1000–5000	80	0.48–0.83	17.3	Hosseinipour et al. [44]
	2000–5000	70	0.6	1	Davies et al. [47]
Semi-batch RO	98–197[a]	90	0.42	97	Efraty et al. [52][b]
	Not reported[c]	80 and 88	0.82 and 0.8	586 and 840	Efraty [17]
	Not reported[d]	82.9	0.94	737	Efraty [53]
Multiple stage RO	5000	91–95	15.8–20.9	6	Cingolani et al. [58]
	900	72	0.71	2595	Kahraman et al. [54]
	2450	71	1.89	1584	Aljundi [59]
New RO technologies (COMRO-OARO)	50,000	75	15	156	Hyrec [57]
	41,000	75	7.4	307	Martinez et al. [30]

[a] Total NO_3 concentration.
[b] Plug flow desalination (PFD)-Semi-batch RO.
[c] Salinity of 6800 and 4000 μS/cm.
[d] Salinity of 6800 μS/cm.

plating wastewater where pressures up to 120 bar are needed. In such applications, the system will recover both water and valuable minerals. In the electroplating wastewater treatment application, a high recovery is needed (>65 %) and both concentrate and permeate streams are reused in the electroplating process resulting in no discharge or waste thus meeting the objectives of a ZLD system. The high-pressure (up to 120 bar) design of HSBRO has now been constructed by the authors at the University of Birmingham and the detailed results will be reported in a forthcoming paper.

The structure of this paper is as follows. Section 2 explains the description and working principles of the HSBRO system. Section 3 describes the improvements made to the mathematical models for the HSBRO system. Section 4 describes the experimental procedures using brackish water as the feed. Section 5 presents the results from the experiments, and discusses the findings of experiments and validation of the mathematical model. Section 6 discusses the results and compares them against other experimental studies reported in the literature. Moreover, in Section 6, the validated model is used to predict system performance at higher pressures and higher salinities. Section 7 summarizes major findings of this study regarding the modelling and experimental results.

2. Operating principle of HSBRO system

Hybrid semi-batch/batch reverse osmosis (HSBRO) operates cyclically over three consecutive phases: 1) semi-batch pressurization, 2) batch pressurization, and 3) purge-and-refill — as shown in Fig. 1.

The process starts with a preliminary purge-and-refill phase, used only in the first cycle to purge any retained salt from previous operations and ensure that the piston starts at the left end of the work exchanger. This prepares the system for the pressurization phases. During the semi-batch pressurization phase (Fig. 1a) the brine valve is closed (off) while the bypass and recirculation valves are open (on). The free piston remains at the left of the work exchanger with no pressure driving it, since the bypass valve is open. The supply pump feeds the system and provides adequate pressure to overcome the osmotic pressure of the feed solution. Permeate is thus produced, while the concentrated brine stream exiting the RO module is recirculated, mixed with the incoming feed, and sent back to the RO module. As salt is added steadily to the system via the feed, concentration and pressure increase linearly with time. The switch point to the next phase can be set either according to a fixed time duration or according to a threshold pressure.

For the next phase (i.e., batch pressurization) the bypass valve is shut while the other valves remain unchanged (Fig. 1b). Now, unlike in the previous phase, there is no mixing between the incoming feed and recirculation stream. The free piston transfers the high pressure generated by the supply pump to the batch volume of water on the right side of the piston. Permeate is produced from the RO module while the concentrated stream is recirculated to the work exchanger by the recirculation pump. In this phase, the concentration inside the system increases at a higher and increasing rate in comparison to the semi-batch pressurization phase. When the piston reaches the right end of the work exchanger, batch pressurization finishes, and purge-and-refill begins.

During the purge-and-refill phase (Fig. 1c), the recirculation valve is closed, while the brine and bypass valves are open. Because the brine valve vents into the atmosphere, the internal pressure drops and water production ceases. Through the bypass and brine valves, the supply pump purges the remaining brine inside the RO module from the system and replaces it with fresh feed water. Purging ends when a volume approximately equal to the volume of water inside the RO module and connecting pipes is flushed out. The end of the refill is detected by zero flow rate through the recirculation pump, indicating that the piston has returned to the left end and cannot move any further.

For further explanation of the rationale and operating principle of the HSBRO system, the reader is referred to reference [15].

3. Theory

A recent study successfully modelled and validated the performance of a batch RO system, including the effect of osmotic backflow which had not been considered previously [44]. This current study extends that approach to the hybrid system, by including also the initial semi-batch phase preceding the batch pressurization phase. The assumptions and equations mostly resemble those used earlier by Park et al. to model the hybrid system [15]; however, the current study uses an analytical rather than numerical approach to solving the equations.

The approach to modelling salt retention has also been improved here. Salt retention determines the initial concentration at the beginning of each pressurization phase and is thus important for the calculation of energy consumption. The above two studies assumed an ideal 100 % rejection in the salt retention calculation, thus ignoring the effect of salt loss across the membrane. Incorporation of a non-ideal salt rejection value (<100 %) means that a lower salt retention is calculated, thus giving a more accurate prediction of *SEC* in the hybrid system.

Because several aspects of the modelling were covered in previous works [15,44], this theory section covers mainly the new aspects. Further details may be found in the Supporting Information (SI).

3.1. Salt retention model

In semi-batch and batch RO generally, salt retention increases the initial osmotic pressure of the solution, resulting in higher energy demand and decreased energy saving compared to conventional RO [44,50]. This phenomenon also affects the hybrid system. To avoid salt retention completely, prolonged purging would be needed between cycles, which would waste feedwater and therefore conflict with achieving

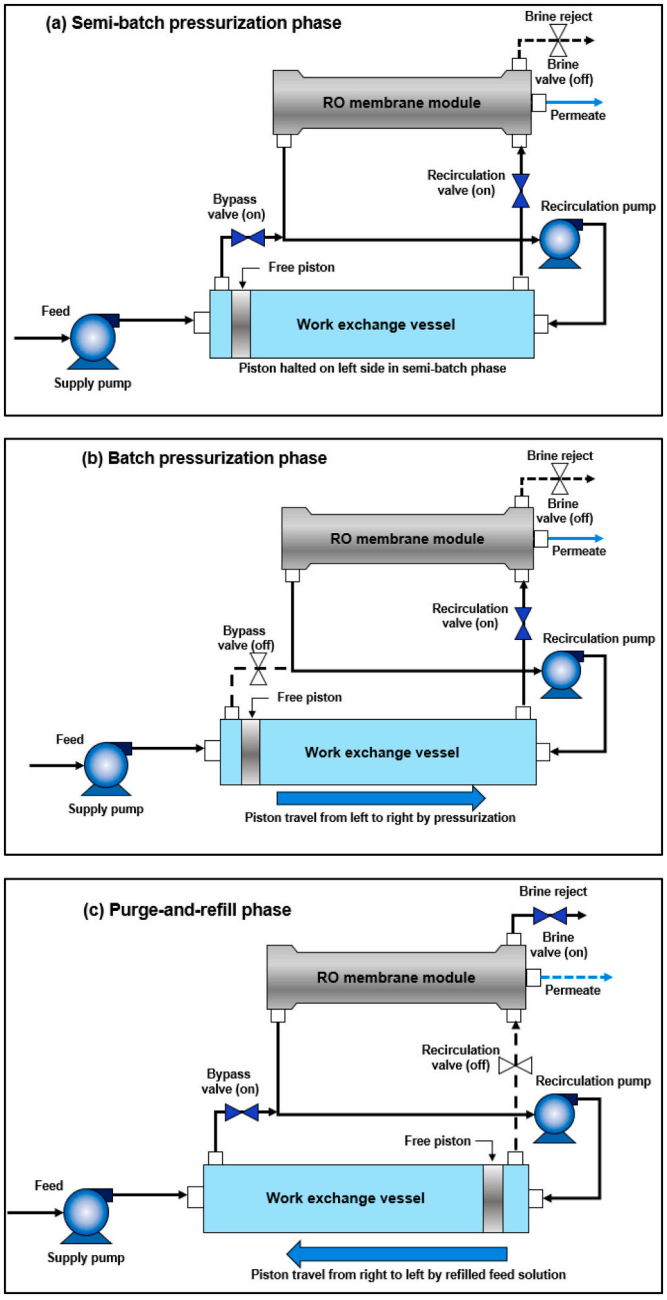

Fig. 1. Hybrid semi-batch/batch reverse osmosis (HSBRO), showing the three phases of cyclic operation. Flow and no flow are depicted by solid and dashed lines, respectively.

higher recovery.

Salt retention S_R refers to the initial concentration in the system at the start of the cycle divided by the feed concentration. Calculation of S_R requires two steps: (1) external mass balance followed by (2) internal mass balance. In the first step, the system is considered as a control volume such that the mass inputs and outputs are balanced at the system boundary over the whole cycle (Fig. 2A). This first step is identical for semi-batch, batch, and HSBRO systems.

Assuming a constant density of the solution, the input volume equals the total output volume i.e.,

$$V_{feed} = V_{permeate} + V_{brine} \quad (1)$$

where V indicates the volume of each stream crossing the boundary (feed, permeate or brine respectively).

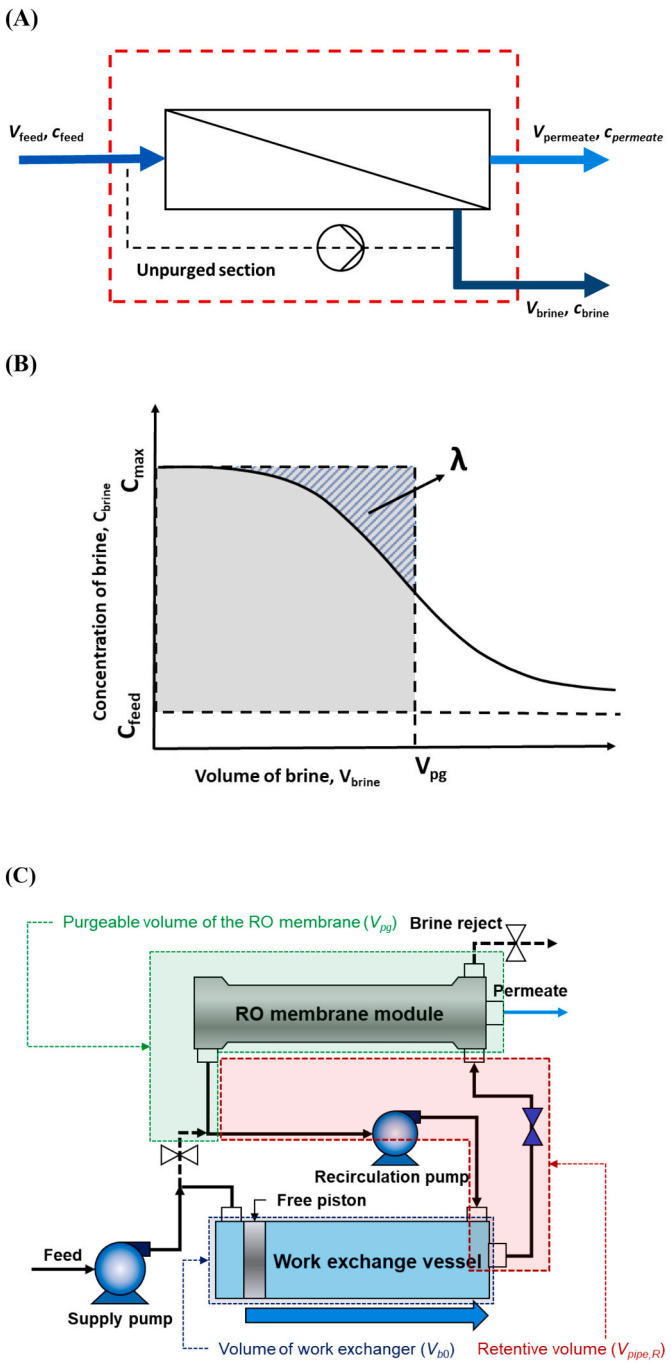

Fig. 2. (A) Sketch of RO system (semi-batch, batch or HSBRO) relevant to external mass balance. The dashed red line shows the system boundary. The unpurged section indicates pipe sections which are not in the purge path, and therefore contribute substantially to salt retention. (B) Concentration at brine outlet vs brine volume during purging, showing longitudinal dispersion parameter λ. This parameter represents the ratio of the hatched area over the larger rectangular area shaded in grey — it remains approximately constant over a range of concentrations and flow conditions. (C) Details of the HSBRO and labelling of volumes, as needed for the analysis of salt retention and recovery. (For interpretation of the references to colour in this figure legend, the reader is referred to the web version of this article.)

By definition, the recovery r is the amount of permeate per amount of feed:

$$r = \frac{V_{permeate}}{V_{feed}} \quad (2)$$

After several cycles, the system reaches a steady repetitive condition regarding concentrations c. Then, over each complete cycle, there is no accumulation of salt inside the system, such that input and output mass of salt balance. Accordingly:

$$V_{\text{feed}}c_{\text{feed}} = V_{\text{brine}}c_{\max} - V_{\text{brine}}\left(c_{\max} - c_{\text{feed}}\right)\lambda + V_{\text{permeate}}c_{\text{permeate}} \tag{3}$$

The first term on the right-hand side is the output of salt that would occur in the absence of dispersion in the RO module. The next term represents salt retained due to dispersion, shown in terms of the maximum concentration $c_{\max}$ and the longitudinal dispersion parameter λ (retained salt as a fraction of the salt that could be purged from the module after purging indefinitely with the feed solution [60]). The last term is the salt leaving via the permeate, where its concentration is c_{permeate} which, in terms of the system rejection R_s, is given by:

$$c_{\text{permeate}} = (1 - R_s)c_{\text{feed}} \tag{4}$$

Eq. (3) shows that a larger value of λ requires a larger maximum brine concentration $c_{\max}$ to balance with the salt fed into the system. In other words, more dispersion results in higher salt retention (see Fig. 2B).

Substituting $V_{brine} = V_{feed} - V_{permeate}$ from Eq. (1) into Eq. (3), and dividing through by V_{feed} and by c_{feed}, gives (using also Eqs. (2) and (4)):

$$1 = (1 - r)\left(\frac{c_{\max}}{c_{\text{feed}}}\right) - (1 - r)\left(\frac{c_{\max}}{c_{\text{feed}}} - 1\right)\lambda + (1 - R_s)r \tag{5}$$

This can be rearranged as:

$$\frac{c_{\max}}{c_{\text{feed}}} = \frac{1 - \lambda(1 - r) - (1 - R_s)r}{(1 - r)(1 - \lambda)} \tag{6}$$

In the second step, the internal mass balance applies to the recirculation loop during the two pressurization phases (but excluding the purge-and-refill phase). It equates the net mass of salt supplied to the mass accumulated in this loop, taking into account the decrease in loop volume:

$$V_{\text{sb}}c_{\text{feed}} - V_{\text{permeate}}c_{\text{permeate}} = \left(V_{\text{pg}} + V_{\text{pipe,R}}\right)c_{\max} - V_0 c_0 \tag{7}$$

where V_{sb} is volume supplied during the initial semi-batch phase, c_0 is the initial concentration and V_0 is the initial volume of the system, given by:

$$V_0 = V_{\text{b0}} + V_{\text{pg}} + V_{\text{pipe,R}} \tag{8}$$

where V_{b0} is the volume of the work exchanger (i.e., the volume supplied during the batch phase), V_{pg} is the purgeable volume of the RO module (including connecting pipes and ports) and $V_{\text{pipe,R}}$ is the retentive volume of the pipework connected to the work exchanger vessel (i.e. the volume that is not in the purge path). Refer to Fig. 2C for explanation of the volumes in the HSBRO system.

Earlier experiments have shown that the volume of permeate collected is equal to the total volume supplied during pressurization, minus the backflow (V_{back}) [44]:

$$V_{\text{permeate}} = V_{\text{sb}} + V_{\text{b0}} - V_{\text{back}} \tag{9}$$

Dividing Eq. (7) by c_{feed}, and substituting from Eqs. (4), (8) and (9), leads to the following expression for salt retention:

$$S_R = \frac{c_0}{c_{\text{feed}}} = \frac{1}{V_0}\left[\left(V_{\text{pg}} + V_{\text{pipe,R}}\right)\frac{c_{\max}}{c_{\text{feed}}} + (V_{\text{sb}} + V_{\text{b0}} - V_{\text{back}})(1 - R_s) - V_{\text{sb}}\right] \tag{10}$$

To calculate S_R, therefore, the value of $c_{\max}/c_{\text{feed}}$ is calculated from Eq. (6) and substituted in Eq. (10).

The above yields the initial concentration c_0, but it is also important to know the concentration c_1 at the end of the semi-batch pressurization (i.e., the beginning of the batch pressurization phase). For this purpose, the internal mass balance is applied to the semi-batch pressurization phase only. The result is similar to Eq. (7), but with the loop volume remaining constant:

$$V_{\text{sb}}c_{\text{feed}} - V_{\text{sb}}c_{\text{feed}}(1 - R_s) = V_0(c_1 - c_0) \tag{11}$$

Rearranging, and substituting for c_0 in terms of S_R, gives:

$$c_1 = c_{\text{feed}}\left[S_R + \frac{V_{\text{sb}}}{V_0}R_s\right] \tag{12}$$

Eq. (12) shows that, unlike in the case of the batch pressurization stage, the salt retention does not have a multiplicative effect on concentration and pressure throughout the semi-batch pressurization phase. Salt retention is important for the initial concentration but has less effect on the final concentration in this phase.

Note that, in this analysis, a uniform value of rejection R_s has been used over the cycle whereas, in fact, it may vary. This approximation is useful to minimize the number of input parameters in the model but could be revised in future works.

3.2. Recovery and backflow

Considering that backflow subtracts from the permeate output, the recovery for the whole system becomes:

$$r = \frac{\text{permeate output}}{\text{feed input}} = \frac{V_{\text{sb}} + V_{\text{b0}} - V_{\text{back}}}{V_{\text{sb}} + V_{\text{b0}} + \left(V_{\text{pg}} - V_{\text{back}}\right)} \tag{13}$$

where V_{sb}, V_{b0} and $V_{\text{pg}} - V_{\text{back}}$ are, respectively, the amount fed in the semi-batch, batch and purge-and-refill phases. Previous work showed that it was appropriate to limit the feed during the purge-and-refill stage, to compensate for backflow; hence V_{back} is subtracted in the last term. Previous experiments [44] showed that, except at very low concentrations, $V_{\text{back}} = 5$ L with an 8-inch RO module and this value is therefore used here.

3.3. Energy consumption

Hydraulic *SEC* is calculated as the hydraulic energy consumption (E) divided by the permeate output (with V_{back} subtracted). For one complete cycle, E is broken down by phase of operation (i.e., semi-batch pressurization, batch pressurization, and purge-and-refill) giving components of E_{P1}, E_{P2} and $E_{\text{P\&R}}$ respectively. Similarly, *SEC* is broken down as follows:

$$SEC = \frac{E}{V_{\text{sb}} + V_{\text{b0}} - V_{\text{back}}} = \frac{E_{\text{P1}} + E_{\text{P2}} + E_{\text{P\&R}}}{V_{\text{sb}} + V_{\text{b0}} - V_{\text{back}}} = SEC_{\text{P1}} + SEC_{\text{P2}} + SEC_{\text{P\&R}} \tag{14}$$

where

$$SEC_{\text{P1}} = \frac{E_{\text{P1}}}{V_{\text{sb}} + V_{\text{b0}} - V_{\text{back}}}, SEC_{\text{P2}} = \frac{E_{\text{P2}}}{V_{\text{sb}} + V_{\text{b0}} - V_{\text{back}}}, SEC_{\text{P\&R}} = \frac{E_{\text{P\&R}}}{V_{\text{sb}} + V_{\text{b0}} - V_{\text{back}}} \tag{15}$$

For each phase, *SEC* can be further broken down between the supply pump and recirculation pump contributions. Using the corresponding subscript for each pump:

$$SEC_{\text{P1}} = SEC_{\text{P1,supply}} + SEC_{\text{P1,recirc}} \tag{16}$$

$$SEC_{\text{P2}} = SEC_{\text{P2,supply}} + SEC_{\text{P2,recirc}} \tag{17}$$

$$SEC_{\text{P\&R}} = SEC_{\text{P\&R,supply}} + SEC_{\text{P\&R,recirc}} \tag{18}$$

The hydraulic energy consumption is calculated as the product of differential pressure and pumped volume V, i.e.

$$E = \int PdV = \overline{P}\Delta V \tag{19}$$

where $\overline{P}$ is the differential pressure averaged over the phase (when P is constant, as is the case during the purge-and-refill phase, no averaging is needed). Pressure is needed to overcome osmotic pressure and to compensate for frictional losses related to the membrane, pipework, and the piston seal. Major pressure terms occur in the pressurization phases. During the semi-batch pressurization phase, concentration and pressure increase linearly as feed is supplied to the system [9] such that the average osmotic pressure is determined by the average of the initial and final concentrations which, using Eq. (12), is given by:

$$\overline{c} = c_{\text{feed}}\left(S_{\text{R}} + \frac{V_{\text{sb}}}{2V_0}R_{\text{s}}\right) \tag{20}$$

With other losses included, the expression for total average pressure required of the supply pump becomes

$$\overline{P_1} = S_{\text{p}}S_{\text{L1}}R_{\text{S}}\pi_{\text{feed}}\frac{\overline{c}}{c_{\text{feed}}} + \frac{J_{\text{w}}}{A_{\text{w}}} - \frac{1}{2}\Delta P_m + \Delta P_{V1} \tag{21}$$

where J_{w} is the water flux through the membrane, A_{w} is the membrane water permeability, ΔP_{m} is the cross-flow pressure drop in the RO module, which is calculated using the correlation of Haidari et al. [61]; S_{p} is the concentration polarization factor calculated as in [62]; and ΔP_{V1} is the pressure drop across the bypass valve which is calculated by the Toricelli equation using a discharge coefficient C_{d}, as in [44]. During batch pressurization, the pressure increases at an increasing rate such that a simple average can no longer be used. Instead, integration under the relevant pressure-volume curve gives [46]:

$$\overline{P_2} = S_{\text{p}}S_{\text{L2}}R_{\text{S}}\pi_{\text{feed}}\frac{c_1}{c_{\text{feed}}}\frac{1}{r_{\text{p}}}ln\frac{1}{1-r_{\text{p}}} + \frac{J_{\text{w}}}{A_{\text{w}}} + \frac{\Delta P_{\text{m}}}{2} + \Delta P_{\text{V2}} + \Delta P_{\text{S}} \tag{22}$$

Note that Eqs. (21) and (22) rely on the assumption of linear correlation between concentration and osmotic pressure (i.e., van't Hoff approximation). This linear assumption is accurate for the brackish water concentrations used in the experiments of this study but may be reconsidered in future works covering higher concentrations or differing feed compositions.

The terms ΔP_{V2} and ΔP_{S} are the pressure drop across the recirculation valve and piston seal respectively; and the pressurization recovery r_{p} is given by:

$$r_{\text{p}} = \frac{V_{\text{b0}}}{V_{\text{b0}} + V_{\text{pg}} + V_{\text{pipe,R}}} \tag{23}$$

The multiplier R_{s} in Eq. (22) is used to account for the concentration on the permeate side, due to finite salt rejection, which lowers the salt gradient and differential osmotic pressure to be overcome. The term S_{p} is the concentration polarization factor, which is calculated exactly as previously [44]. The terms S_{L1} and S_{L2} are the longitudinal concentration factors in the semi-batch and batch pressurization phases respectively, which are calculated based on ordinary differential equation (ODE) models. The model used for S_{L1} is new, and included in the SI section 4. The model for S_{L2} is the same as that used previously for the non-hybrid batch RO process [46]. As such, the model for S_{L2} assumes uniform concentration at the start of the batch RO pressurization phase. In fact, the concentration would be slightly non-uniform according to the conditions reached during the preceding semi-batch pressurization phase. Nonetheless, this simplifying assumption is preferred, as it allows the energy contribution of each phase to be modelled independently.

For the purge-and-refill phase, only minor frictional losses are encountered, including the losses in valves and piston seal friction. The corresponding calculations are included in the SI section 1, which explains in detail the flow paths and pressure drops for each pump and phase of operation.

The above calculations give the hydraulic *SEC*. The electrical *SEC* equals the hydraulic *SEC* divided by the overall pump efficiency (i.e. the efficiency of the pump and electric motor).

3.4. Peak pressure

Finally, the peak pressure at the end of the batch pressurization phase is calculated as in reference [46], but taking into account the elevated concentration c_1 at the start of this phase and salt rejection R_{S}:

$$\widehat{P} = S_{\text{p}}R_{\text{S}}\pi_{\text{feed}}\frac{c_1}{c_{\text{feed}}}\frac{1}{1-r_{\text{p}}} + \frac{J_{\text{w}}}{A_{\text{w}}} + \frac{\Delta P_{\text{m}}}{2} + \Delta P_{\text{V2}} + \Delta P_{\text{s}} \tag{24}$$

3.5. Second law efficiency

Second law efficiency is useful for comparing desalination systems working at different feed salinities and recoveries. It is defined as the ideal *SEC* divided by that really obtained.

The ideal *SEC* corresponds to the change in Gibbs energy between the inlet and outlet streams. For a generalized desalination system treating a dilute solution [63], this is given by:

$$SEC_{min} = \pi_{\text{feed}}\left[\frac{1}{r}ln\left(\frac{1-r[1-R_s]}{1-r}\right) - (1-R_{\text{S}})ln\left(\frac{1-r[1-R_s]}{(1-r)(1-R_s)}\right)\right] \tag{25}$$

3.6. Concentration factor (*CF*)

Concentration factor refers to the concentration of the brine divided by that of the feed. It is related to the recovery and rejection of the RO system by:

$$\text{CF} = \frac{1-r[1-R_s]}{1-r} \tag{26}$$

4. Experimental

4.1. Experimental equipment

The HSBRO system investigated in this study is the same as described in [44]. Only the sequence of valve operation is modified. Fig. 3 shows a schematic of the HSBRO prototype.

The system uses a single-acting free piston and an 8-inch RO module to obtain an output up to 22 m^3/day. Experiments were conducted using an Eco Pro-440 membrane element (Dupont) with 41 m^2 active area. The output is limited by the maximum operating pressure of 25 bar, which limits the flux J_{w} to about 24 L/m^2/h with this membrane. Major parts include two pumps (supply and recirculation pumps), three motorized on-off valves, two pressure vessels (one housing the free piston and the other an 8-inch RO membrane) and nine sensors to measure pressures, flow rates and conductivities. A stainless-steel housing holding a 10-inch length cartridge filter (5 μm pores) is also used to remove the particulates inside the feed water for membrane protection. Additionally, a one-way valve installed on the permeate outlet reduces backflow when the system depressurizes at the end of the batch pressurization phase. SI section 2 includes details of parts and instruments used, as well as constant parameters of the system.

The system is controlled by a Programmable Logic Controller (PLC) which uses timers and feedback from pressure, flow, and conductivity sensors to control the pumps and the valves. The PLC program can be adjusted to achieve the desired recovery at various water fluxes. The recovery was determined by dividing the mass of water collected in the permeate tank, by the mass of water leaving the feed tank.

4.2. Experimental procedure

To evaluate the HSBRO performance, a series of experiments were carried out at various feed salinities and water permeate fluxes, at recovery $r \geq 0.94$. Because the system was designed for brackish water treatment, its operating pressure was limited to 25 bar. We therefore used feed solutions with maximum concentration of 1500 mg/L to avoid exceeding this limit. Thus, concentrations of 500, 1000, and 1500 mg/L

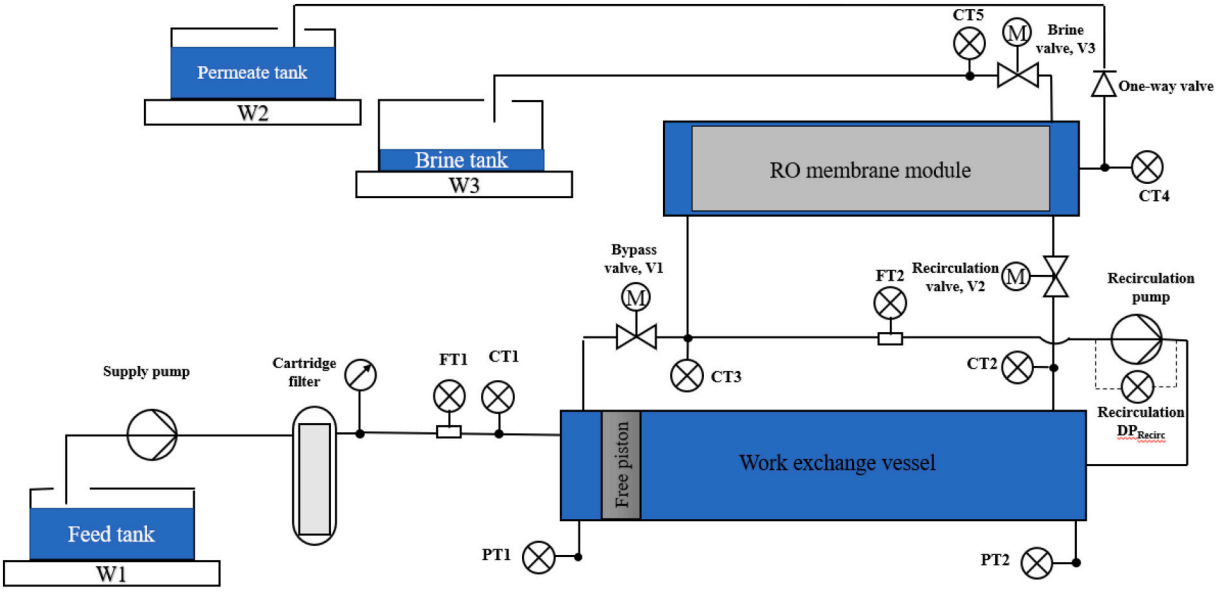

Fig. 3. Schematic diagram of high-recovery hybrid semi-batch/batch RO (HSBRO) system (PT, CT and FT are pressure, conductivity and flow transmitters, respectively; W1, W2, and W3 are weighing platforms for feed, permeate and brine tanks; M indicates motorized valves).

and water permeate fluxes of 10–24 L/m^2/h were selected. These concentrations corresponded to conductivities of 1.019, 1.995 and 2.945 mS/cm respectively (see SI section 5 for conversion factors from conductivity to concentration).

The feed solution was prepared using tap water (salinity of ~100 mg/L) and analytical grade sodium chloride (purity>99.5 %). 4.5 mg/L of sodium metabisulfite (SMBS) was also added to the feed tank to counteract free chlorine in the tap water and prevent membrane oxidization. Experiments were conducted at a constant temperature (25 °C) maintained by a thermostatic immersion heater. An external mixing pump was used to homogenize the water inside the feed tank before and during the tests.

Because of salt retention, initial cycles gave a different pattern of concentration vs. time. After two cycles the system stabilized; thus, we took the third cycle as representative of continued operation. All the parameters including time, supply and batch pressure, conductivities in supply, entry to the RO module, the exit of the RO module, brine, and permeate streams, differential pressure of the recirculation pump, electrical energy consumption of both supply and recirculation pumps, and weight of the feed, permeate and brine tanks were recorded at a frequency of at least once per second, resulting in at least 3000–8000 sets of readings per cycle. The raw data files are indexed in the SI section 5 and included as electronic appendices. These data were used to calculate results such as hydraulic and electrical *SEC*, recovery, rejection, and concentration factor and thus evaluate system performance.

5. Results

5.1. Salt retention

Salt retention has an important influence on the initial salt concentrations c_0 and c_1 at the start of the semi-batch and the batch pressurization phases respectively. According to the theory above, the concentration should increase linearly from the c_0 to c_1 as predicted by Eqs. (10) and (12). To verify the theory, Fig. 4 presents the experimental and theoretical variations of salt concentration (measured at the inlet of the RO module) from the start to the end of the semi-batch pressurization phase. Experiments were conducted at 1000 mg/L feed concentration and J_w = 18.9 L/m^2/h. Except for some initial fluctuation in concentration, there was good agreement between experimental measurements and theoretical values.

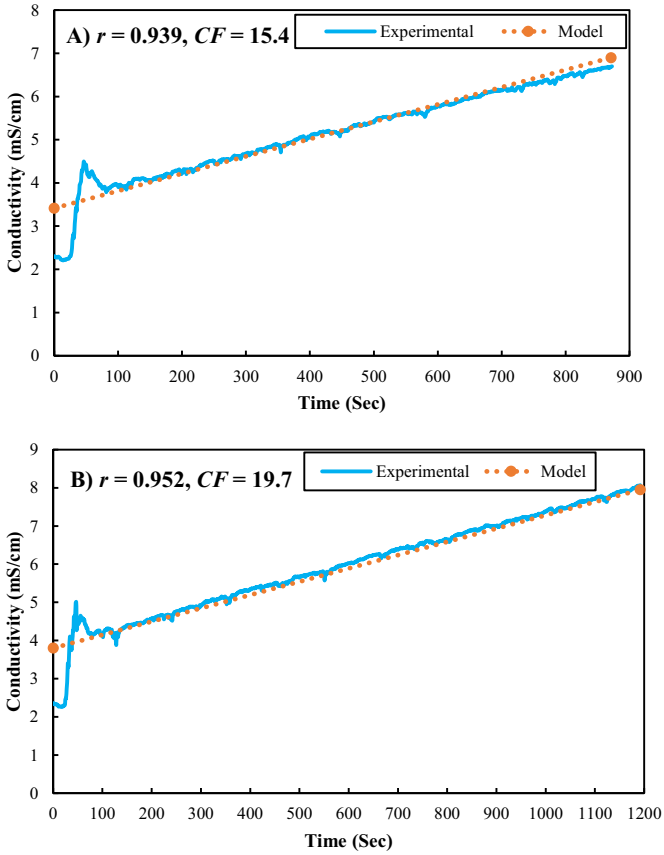

Fig. 4. Comparison of model predictions and experimental inlet conductivity into the RO module vs. time in semi-batch pressurization phase at feed salinity c_{feed} = 1000 mg/L, flux J_w = 18.9 L/m^2/h, A) recovery r = 0.939 and concentration factor CF = 15.4, B) recovery r = 0.952 and concentration factor CF = 19.7. See SI section 5 for conversion between conductivity and concentration.

The above theory and experiments correspond to the case where the purged brine volume V_{brine} (collected at the outlet) equals the purgeable volume V_{pg} of the batch RO system. But it is also interesting to study the

case of smaller or larger brine volumes during purging. For this purpose, we carried out some tests to measure the salt retention inside the HSBRO system over a range of V_{brine}/V_{pg}. These tests were conducted at 1000 mg/L feed salinity, and $J_w = 18.9$ L/m^2/h. At each value of V_{brine}/V_{pg}, the system was operated for three cycles. Once the third cycle purge-and-refill phase had finished, we mixed the water inside the whole system (including membrane and work exchanger) for 10 min using the recirculation pump and then measured the solution concentration and divided it by the feed concentration to calculate the salt retention ($S_R = c_0 / c_{feed}$).

Fig. 5 demonstrates the effects of varying purged brine volume on salt retention and recovery. At $V_{brine}/V_{pg} = 1$ (i.e. brine volume equal to the purgeable volume of solution inside the membrane and pipes) and $r = 0.94$, salt retention was 1.89 ± 0.03, slightly higher than the theoretical prediction of $S_R = 1.78$. As expected, by increasing the purged brine volume, salt retention decreased but at the expense of lower recovery since the permeate production was constant. Therefore, there is a trade-off between either (1) higher recovery and higher salt retention, or (2) lower recovery and lower salt retention. Salt retention dropped substantially on purging more; for example, on increasing V_{brine} from 16.5 ($V_{brine}/V_{pg} = 1$) to 24.6 L ($V_{brine}/V_{pg} = 1.5$), salt retention dropped 24 % from 1.89 to 1.44. Alongside, however, the recovery fell from 0.940 to 0.913. In the case of less purging, salt retention increased sharply. For instance, when $V_{brine}/V_{pg} = 0.9$, salt retention was 2.26 which is 20 % larger than when $V_{brine}/V_{pg} = 1$, while the recovery was only slightly higher at $r = 0.945$ compared to $r = 0.94$.

Electrical *SEC* decreased with increasing purged brine volume. Fig. 6 presents the effect of V_{brine} on the electrical *SEC* at 1000 mg/L feed salinity and $J_w = 18.9$ L/m^2/h. Total electrical *SEC* decreased from 0.502 to 0.468 kWh/m^3 when we increased V_{brine}/V_{pg} from 0.9 to 1.5. As we saw in Fig. 5, longer purge leads to less salt retention, which in turn decreases the applied pressure and energy requirements.

In the non-hybrid batch RO studied previously, we observed almost constant electrical *SEC* over the same range of purged brine volumes [44]. However, in HSBRO we observed about a 7 % decrease in electrical *SEC* at larger volumes. The main reason is that salt retention in HSBRO is much larger than in batch RO (1.89 compared to 1.16 at $V_{brine}/V_{pg} = 1$), and it has a greater effect on energy consumption. As can be seen in Fig. 6, larger purged brine volume caused a reduction in the supply pump *SEC* in both semi-batch and batch pressurization phases, which dominated over the increase during the purge-and-refill phase.

Fig. 7 shows concentration inside the recirculation loop over the semi-batch pressurization phase, for different values of V_{brine}/V_{pg}. As in Fig. 4, concentration increased linearly over time. Smaller amounts of purging ($V_{brine}/V_{pg} < 1$) led to higher initial and final concentrations.

5.2. Hydraulic SEC

The hydraulic energy consumption for each pump was measured by integrating the amount of water transferred by that pump with respect to the differential pressure. The integration was carried out over successive time steps using the trapezoidal rule. Then, experimental hydraulic *SEC* was obtained by dividing the consumed energy by the permeate volume output as measured by the weighing tank (W2). For the model predictions of *SEC*, the model input parameters are included in Table S3. The discharge coefficient of $C_d = 0.62$ is consistent with the range of 0.61 to 0.66 reported for orifices generally [64] and only has a minor influence on the total energy consumption within this range. The dispersion parameter was determined as $\lambda = 0.15$ based on an analysis of exit brine concentration during purge under conditions of osmotic backflow (see SI section 3). Note that this value differs from the previous study, where the influence of osmotic backflow was not rigorously included in the salt retention calculation [44]. The backflow volume was assigned a value of $V_{back} = 5$ L, according to the backflow typically observed in this and the previous study. The piston friction of $\Delta P_s = 3.5$ kPa was observed from measurements of the differential pressure (see SI section 6).

To match the model and experimental results, two important adjustable parameters were used, as follows. The membrane permeability was assigned the same value of $A_w = 4.4$ L/m^2/h/bar as in the previous study [44]. In this new study, the salt rejection was assigned the value of $R_s = 0.94$, consistent with the observed permeate salt concentration.

Fig. 8A compares experimental values of hydraulic *SEC* against the model predictions at different feed salinities for each pump and phase of operation ($r = 0.94$, and $J_w = 18.9$ L/m^2/h). Total experimental hydraulic *SEC* increased with feed salinity from 0.202 to 0.308 kWh/m^3 at 500 and 1500 mg/L respectively. Since recovery and permeate water flux were kept constant at different tested feed salinities, the amount of water displaced by each pump was the same. However, at increased feed salinity, supply pressure increased with osmotic pressure. As a result, the hydraulic *SEC* of the semi-batch and batch pressurization phases

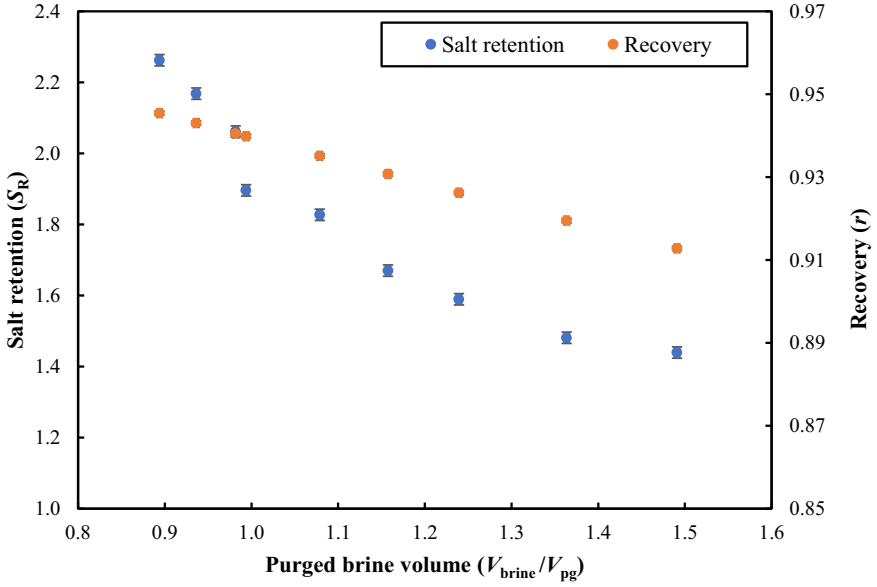

Fig. 5. Observed salt retention and recovery as a function of normalized purge volume at feed salinity $c_{feed} = 1000$ mg/L and flux $J_w = 18.9$ L/m^2/h.

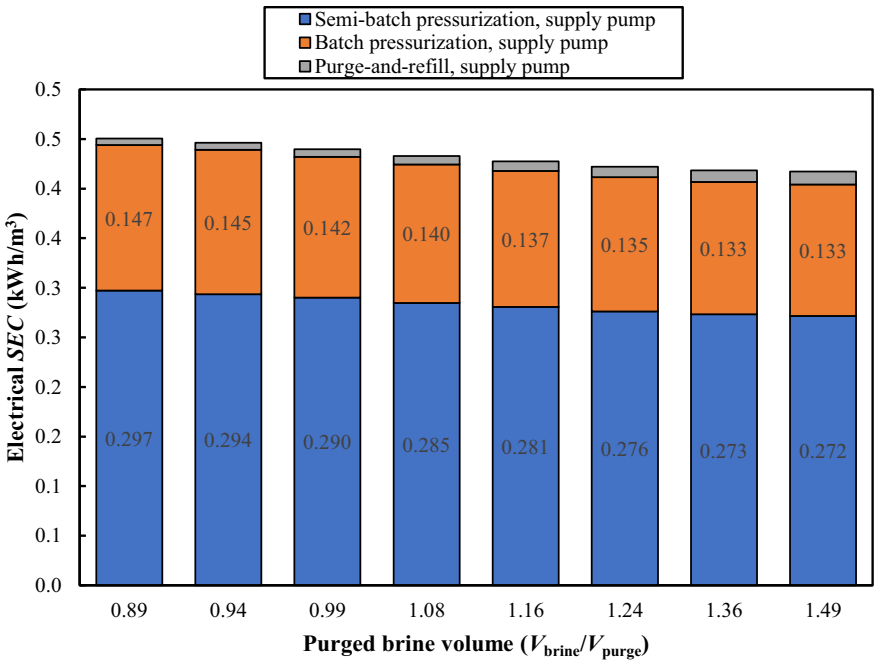

Fig. 6. Electrical *SEC*, supply pump breakdown as a function of normalized purged brine volume at feed salinity c_{feed} = 1000 mg/L and flux J_w = 18.9 L/m^2/h.

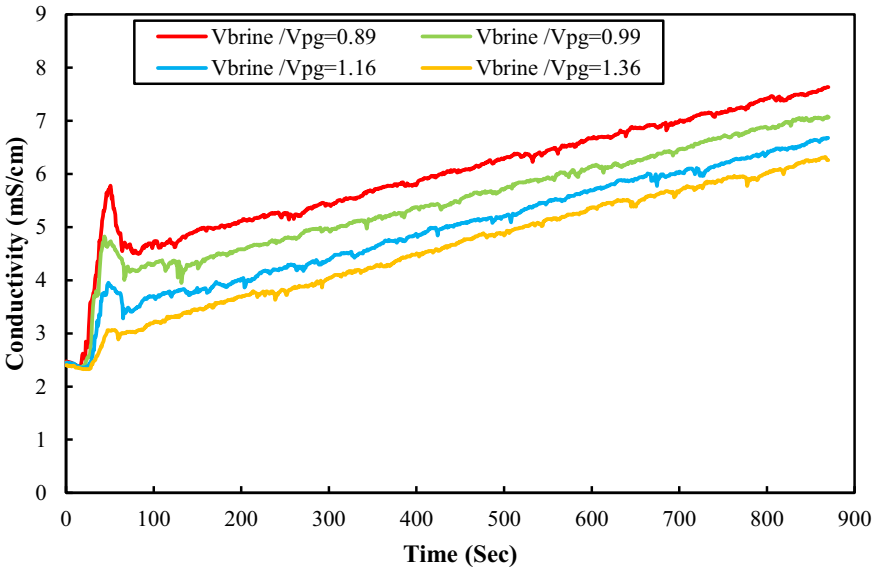

Fig. 7. Effect of varying purge volume on recirculation loop concentration (represented by conductivity) over a semi-batch pressurization phase (r = 0.94, J_w = 18.9 L/m^2/h, c_{feed} = 1000 mg/L). See SI section 5 for conversion between conductivity and concentration.

increased; whereas the energy consumed by both the recirculation and supply pumps during the purge-and-refill phase remained constant. For example, measured supply pump *SEC* during pressurization phases ($SEC_{P1,supply}$ + $SEC_{P2,supply}$) was 0.181, 0.239, and 0.287 kWh/m^3 at 500, 1000, and 1500 mg/L feed solutions respectively, while other *SEC* contributions totalled only 0.021 kWh/m^3 regardless of feed concentration. As expected, most of the energy was consumed by the supply pump during the two pressurization phases. The model predicted well the hydraulic *SEC* (Fig. 8A). The highest error was around 2 % with the 1000 mg/L feed solution while at 500 and 1500 mg/L the error between experimental results and model values was <1 %.

Fig. 8B compares experimental measurements of hydraulic *SEC* against predicted values at various water fluxes, r = 0.94, and 1000 mg/L feed salinity c_{feed}. It shows an increase of hydraulic *SEC* with flux. This is because more pumping pressure was needed to overcome hydrodynamic resistance in the RO membrane pores ($P \propto J_w / A_w$). Thus, the *SEC* of the supply pump over the two pressurization phases, $SEC_{P1,supply}$ + $SEC_{P2,supply}$, increased from 0.187 to 0.28 kWh/m^3 as flux almost doubled from 12.1 to 23.6 L/m^2/h. However, unlike in Fig. 8A, the recirculation pump *SEC* was not constant. To achieve higher permeate flux, we needed to increase the feed flow rate; then to maintain an optimum value of $Q_r/Q_f \approx 2$, we had to increase the recirculation flow rate proportionately which led to an increase in recirculation pump *SEC*. For instance, on increasing water flux from 12.1 to 23.6 L/m^2/h, the experimental recirculation pump *SEC* over the two pressurization phases, $SEC_{P1,recirc}$ + $SEC_{P2,recirc}$, increased from 0.008 to 0.022 kWh/m^3. Overall, by almost doubling the water flux, we observed a 54 % increase in total hydraulic *SEC* from 0.2 to 0.308 kWh/m^3. Fig. 8B also shows

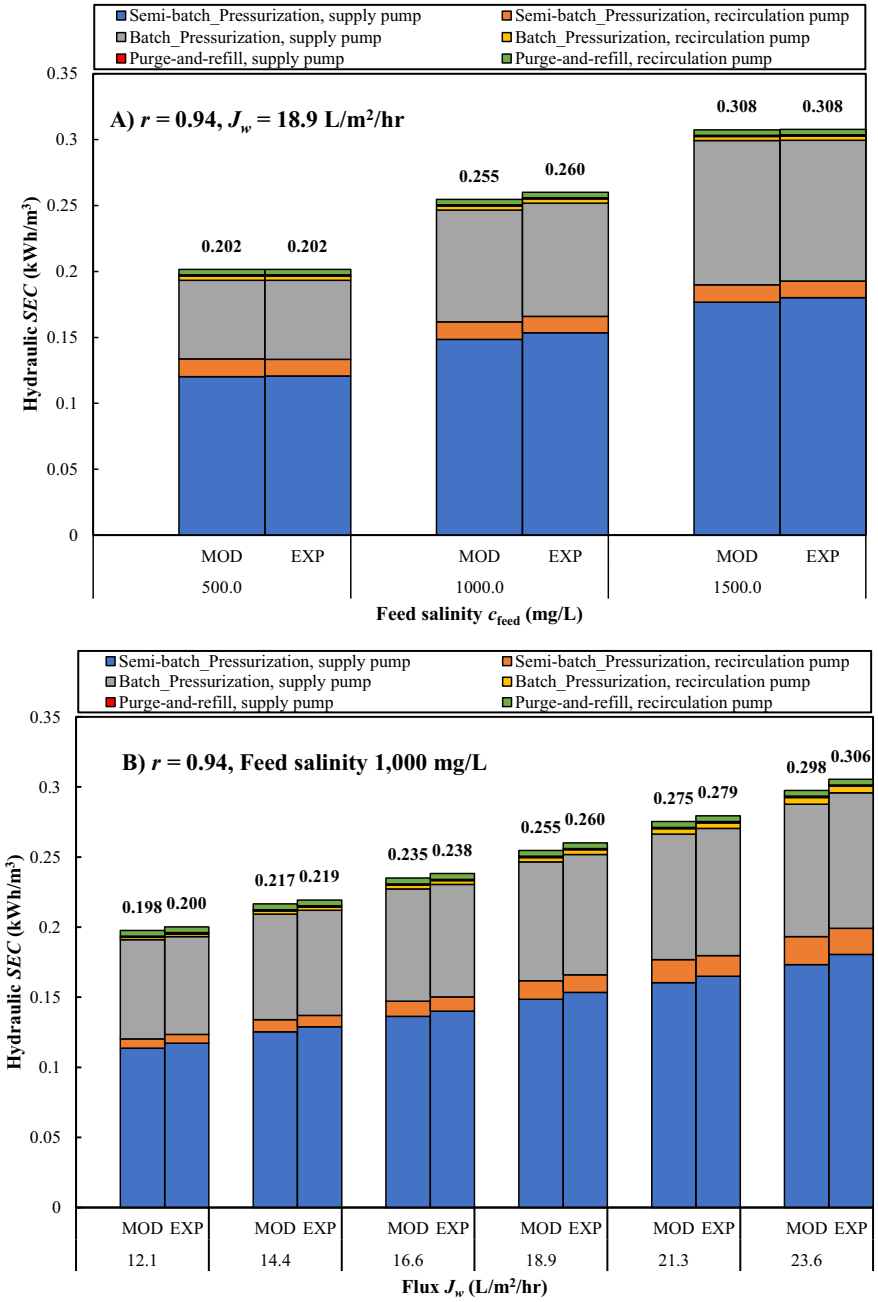

Fig. 8. Comparison of hydraulic *SEC* breakdown between experimental measurements (EXP) and model predictions (MOD) at recovery $r = 0.94$. A) different feed salinities at $J_w = 18.9$ L/m^2/h, and B) different water fluxes at $c_{feed} = 1000$ mg/L.

model predictions of hydraulic *SEC* at different water fluxes. The model again agrees well with the experimental results, with <3 % error.

5.3. Electrical SEC

We calculated electrical *SEC* of the HSBRO system by integrating, over time, the electrical power (current × voltage) consumed by both pumps and then dividing by the amount of permeate water produced.

Fig. 9A compares electrical and hydraulic *SEC* breakdown at different water salinities, at $r = 0.94$ and $J_w = 16.5$ L/m^2/h. As feed salinity increased, both electrical and hydraulic *SEC* increased, but the increase in electrical *SEC* was less marked. At 500, 1000, and 1500 mg/L, total electrical *SEC* was 0.394, 0.458, and 0.501 kWh/m^3 respectively compared to hydraulic *SEC* of 0.181, 0.238, and 0.278 kWh/m^3 with the main contribution coming from the supply pump. Total electrical *SEC* was respectively 118, 92, and 80 % higher than the hydraulic *SEC*. As seen in Table 2, the lower increase in electrical *SEC* was associated with supply pump efficiency increasing from 45.9 to 55.5 % (while the recirculation pump efficiency remained constant at about 35 %).

Fig. 9B compares hydraulic and electrical *SEC* at various water fluxes, at $r = 0.94$ and 1000 mg/L feed concentration. By increasing water flux from 12.1 to 23.6 L/m^2/h, both *SECs* increased: hydraulic *SEC* by 53 % from 0.2 to 0.306 kWh/m^3, and electrical *SEC* by 31 % from 0.419 to 0.549 kWh/m^3. Again, the increase in electrical *SEC* was smaller, because of increased pump efficiency at higher pressures associated with the higher fluxes. As water flux doubled, supply pump efficiency increased by a factor of 1.18 (from 47.7 % to 56.1 %) in semi-batch and by 1.11 (from 57.5 % to 63.9 %) in batch pressurization phases respectively (see Table 3). The recirculation pump *SEC* also increased with flux. Again, electrical *SEC* increased less than hydraulic

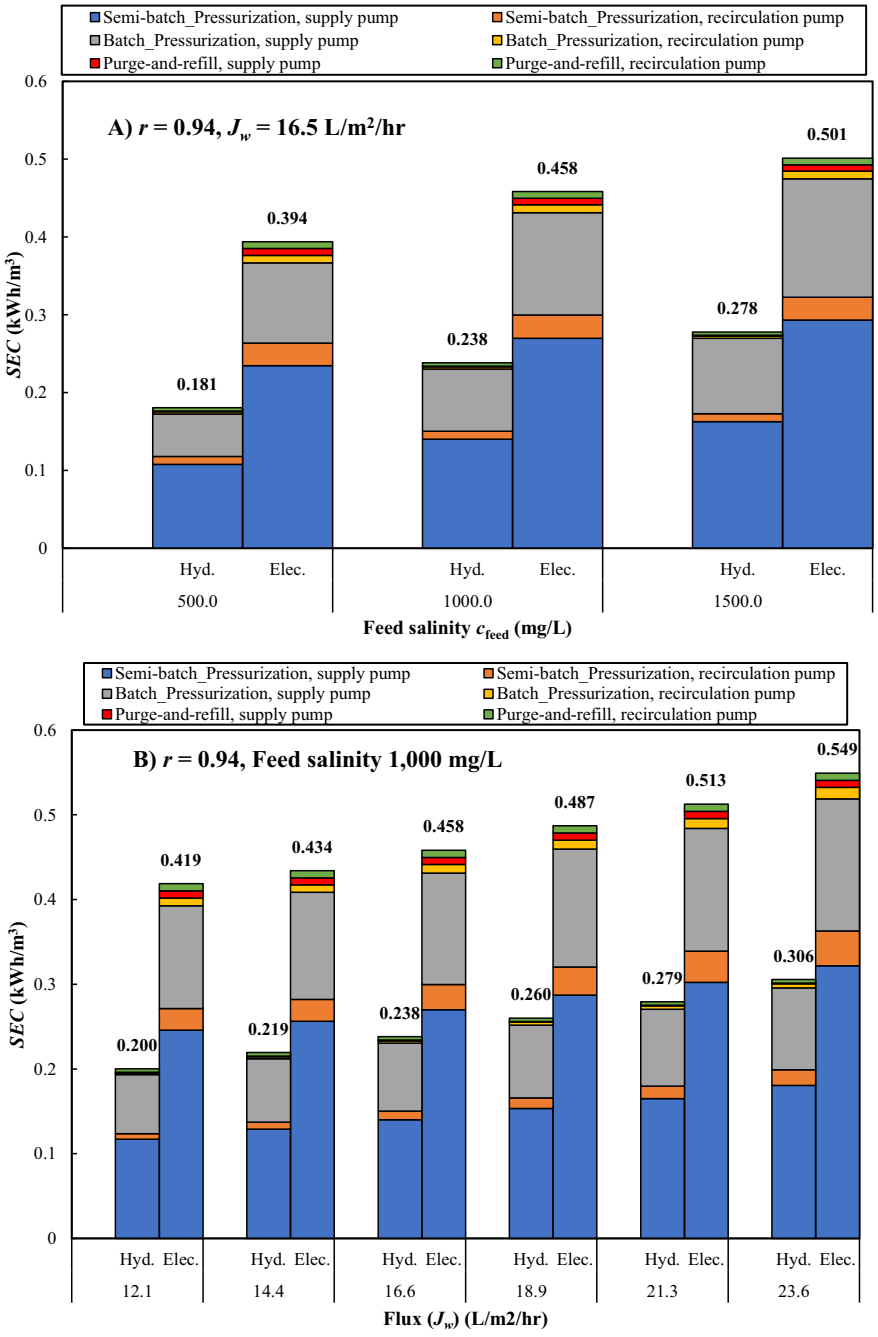

Fig. 9. Comparison of hydraulic and electrical *SEC* breakdown at $r = 0.94$. A) different feed salinities at $J_w = 16.5$ L/m^2/h, and B) different water fluxes at $c_{feed} = 1000$ mg/L.

Table 2
Supply and recirculation pump efficiencies for semi-batch pressurization, batch pressurization, and purge-and-refill phases at various feed salinities (flux $J_w = 16.5$ L/m^2/h).

Feed salinity c_{feed} (mg/L)	Pump efficiency (%)					
	Supply pump			Recirculation pump		
	Semi-batch pressurization	Batch pressurization	Purge-and-refill	Semi-batch pressurization	Batch pressurization	Purge-and-refill
500	45.9	53.2	10.3	35.3	28.3	48.6
1000	51.9	60.9	10.8	34.4	27.3	48.7
1500	55.5	63.9	12.2	34.6	27.3	48.3

Table 3
Supply and recirculation pump efficiencies for semi-batch pressurization, batch pressurization, and purge-and-refill phases at various water fluxes and c_{feed} = 1000 mg/L.

Flux J_w (L/m^2/h)	Pump efficiency (%)					
	Supply pump			Recirculation pump		
	Semi-batch pressurization	Batch pressurization	Purge-and-refill	Semi-batch pressurization	Batch pressurization	Purge-and-refill
12.1	47.7	57.5	12.9	24.5	18.9	47.7
14.4	50.3	59.3	12.4	32.0	24.7	47.6
16.6	51.9	60.9	10.8	34.4	27.3	48.7
18.9	53.4	61.8	10.6	37.7	30.5	48.1
21.3	54.6	62.6	10.9	40.0	33.2	48.3
23.6	56.1	63.9	11.9	42.5	34.4	48.1

SEC because recirculation pump efficiency increased with flow. For example, when flux increased from 12.1 to 23.6 L/m^2/h, we observed an increase in efficiency by a factor of 1.73 (from 24.5 % to 42.5 %) and by 1.82 (from 18.9 % to 34.4 %) during semi-batch and batch pressurization phases respectively (Table 3). However, since the recirculation pump consumes <12 % of total energy, it had a minor impact on total *SEC* in all cases.

Fig. 10 shows the percentage contribution of each pump to the total electrical *SEC* during different phases of operation at different feed salinities, at $r = 0.94$ and $J_w = 18.9$ L/m^2/h. The largest fraction (about 60 %) of electrical *SEC* came from the supply pump during semi-batch pressurization. Over both phases of pressurization, this fraction increased to 86–89 %. The fraction slightly increased with feed salinity, as the absolute contribution from the recirculation pump remained constant. In total, about 10–12 % of *SEC* came from the recirculation pump.

A useful feature of HSBRO is the ability to achieve different recoveries by changing the duration of the semi-batch pressurization phase. Fig. 11 compares electrical *SEC* breakdown at two different recoveries for 500 mg/L feed solution and $J_w = 23.6$ L/m^2/h. At $r = 0.979$, semi-batch pressurization share of *SEC* was around 77 % while this was 59 % at $r = 0.94$. This is because the operation time at $r = 0.979$ was much longer; this increased the concentration inside the system and consequently more pressure was needed. To reach $r = 0.979$, semi-batch duration was 2580 s (about 88 % of cycle time) while for $r = 0.94$ it was 690 s (about 68 % of cycle time). The batch and purge-and-refill durations for both recoveries were about the same at 259 and 76 s respectively. In addition, at $r = 0.94$, the contributions of semi-batch and batch phases to the total recovery were $r_{sb} = 0.704$ and $r_b = 0.236$ respectively, while at $r = 0.979$ these values were $r_{sb} = 0.898$, $r_b = 0.081$. Although, in theory, operating longer at semi-batch mode increases the energy penalty, it reduces the need for having a large work exchanger which becomes impractical at such high recoveries. The unfavourable *SEC* contributions (i.e. purge-and-refill phase, and recirculation pump over pressurization phase) were 12 and 15 % at $r = 0.979$ and $r = 0.94$ respectively. Recirculation pump *SEC* was the same in both cases (11 %) while at higher recoveries the purge-and-refill *SEC* portion was much smaller, around 1 % at $r = 0.979$ compared to 4 % at $r = 0.94$.

5.4. Permeate conductivity changes over a cycle

Fig. 12 shows how permeate quality changed over the semi-batch and batch pressurization phases at $r = 0.94$, $J_w = 21.3$ L/m^2/h, and different feed salinities. At the start of water production, permeate conductivity rose sharply, peaked after 30 s, and dropped quickly. It then increased again slowly as the recirculation stream concentration increased. The initial peak is attributed to salt diffusion after the system depressurizes. During the purge-and-refill phase, the RO module is filled with brine and, due to the concentration gradient, salt continues to pass through the membrane. When the next pressurization phase starts, this salty water leaves in the permeate thus causing this peak.

The pattern was similar to that seen in batch RO [44], but in HSBRO

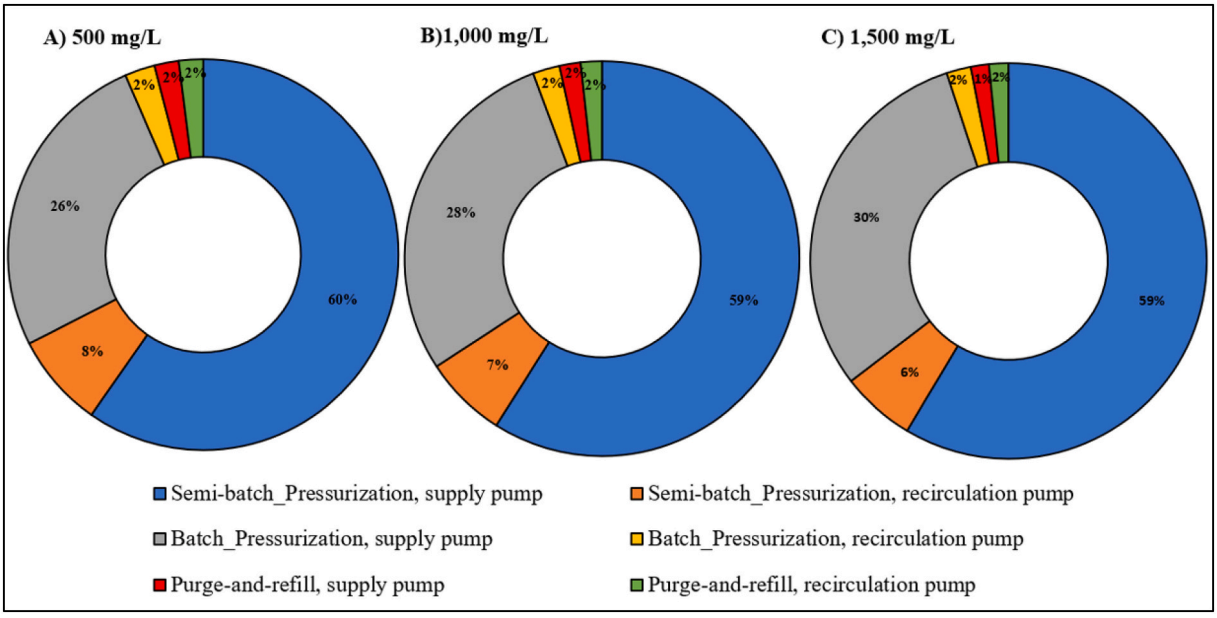

Fig. 10. Percentage contribution of each pump to total electrical *SEC* at each operation phase at feed salinity A) c_{feed} = 500 mg/L, B) c_{feed} = 1000 mg/L, and C) c_{feed} = 1500 mg/L. ($r = 0.94$ and $J_w = 18.9$ L/m^2/h).

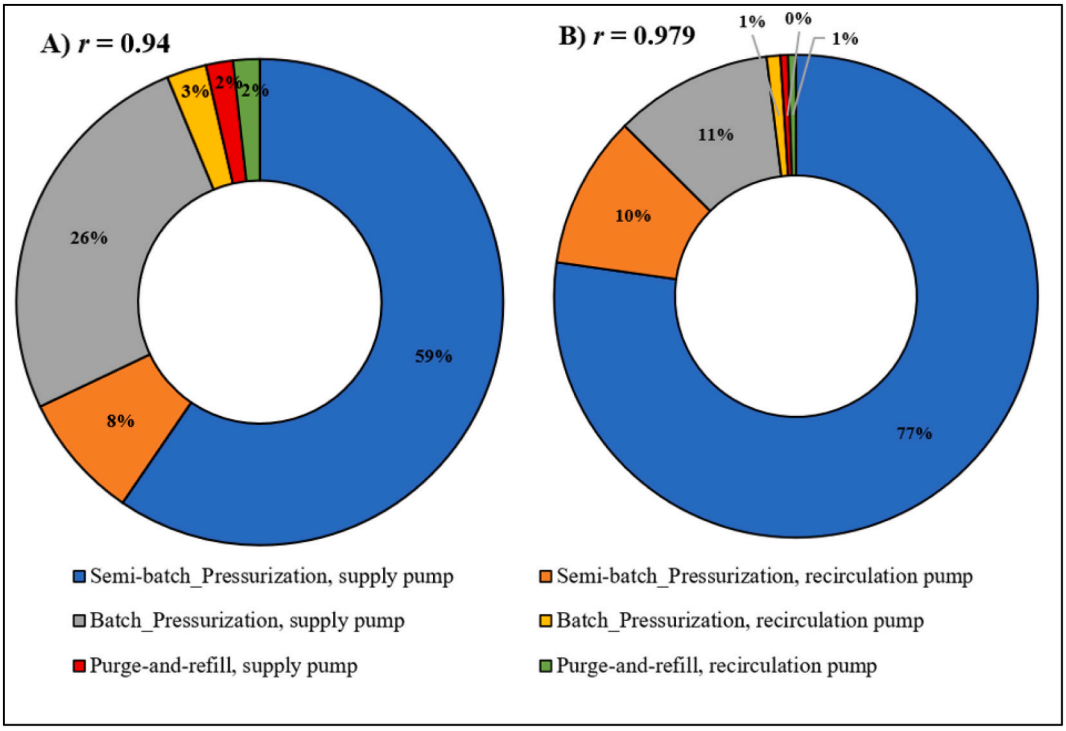

Fig. 11. Percentage contribution of each pump to total electrical *SEC* at each operation phase at feed salinity $c_{feed} = 500$ mg/L, flux $J_w = 23.6$ L/m^2/h, and recovery A) $r = 0.94$, and B) $r = 0.979$.

the peak was higher. For example, at 1000 mg/L feed, in batch RO, conductivity peaked at only 0.3 mS/cm whereas in HSBRO it peaked at around 1.5 mS/cm. This was because of the higher recovery and concentration factor in the HSBRO case, which provided a larger concentration gradient to drive salt passage into the permeate. At 500, 1000 and 1500 mg/L feed concentration, permeate conductivity peaked at around 0.6, 1.5 and 2.0 mS/cm, respectively (Fig. 12A–C). The initial conductivity peak has a detrimental effect on the overall rejection of the system. For instance, in cases A, B, and C (Fig. 12A–C), the rejection was 95.4, 94.3, and 93.9 % respectively. However, if the initial peak had not occurred, rejection would have increased to 96.1, 95.2, and 94.7 % respectively. In another words, salt passage ($1 - R_s$) of the system would have decreased by 15 %.

The rate of permeate conductivity increase in batch mode is higher than semi-batch mode. For example, after the initial peak, permeate conductivity increased from around 0.04 to 0.09 mS/cm in semi-batch while it increased from around 0.09 to 0.43 mS/cm in the batch phase. The reason is that in semi-batch mode the concentration at the entrance of the RO module increased linearly with time, whereas in batch mode it grew at an increasing rate.

5.5. Pressure and conductivity changes over a cycle

Fig. 13 shows variations against time of applied pressure and incoming solution conductivity to the RO module at $r = 0.94$, $J_w = 18.9$ L/m^2/h and feed salinity of 1000 mg/L. Because pressure tends to increase with concentration, these two variables show similar trends over the cycle. In the semi-batch pressurization phase, with an assumption of constant rejection, concentration increases linearly since the internal loop volume is constant while solute is added at a constant rate. Therefore, the permeate that leaves the loop is replaced by the same amount of feed. However, during batch pressurization, the internal loop volume decreases linearly with time while the contained mass of solute remains constant. Consequently, concentration increases at an increasing rate as seen in Fig. 13.

We also compared the experimental peak pressure with the predicted values by the model at different water fluxes, $r = 0.94$, and 1000 mg/L feed salinity (Fig. 14). Predicted values exceeded slightly the experimental results. One possible cause for the discrepancy is membrane deformation and compaction at high pressure. This may lead to increased internal volume, lower concentration, and hence lower final osmotic pressure. Another factor may be the variation in salt rejection which, though considered constant in our model, in fact increases with flux. Higher salt rejection results in higher salt retention, thus increasing the peak pressure and causing the measured peak pressure to approach the predicted value at higher fluxes.

5.6. Recirculation flow optimization

Table 4 shows the effect of recirculation flow Q_r at the brine exit of the RO module, as a ratio to feed flow Q_f, on important parameters including pressurization *SEC* in the HSBRO system. On increasing Q_r/Q_f, recirculation pump *SEC* over the two pressurization phases increased because of the higher flow rate, while the corresponding supply pump *SEC* decreased due to lower concentration polarization and longitudinal concentration gradient. This trend is also shown by the average pressure required for the process, which decreased with Q_r/Q_f. For example, on increasing Q_r/Q_f from 1.5 to 3.7, the average required pressure decreased from 9.08 to 8.23 bar which directly reduced supply pump *SEC* during pressurization by 0.026 kWh/m^3 from 0.441 to 0.415 kWh/m^3; while the corresponding recirculation pump *SEC* increased by 0.124 kWh/m^3 from 0.027 to 0.151 kWh/m^3. Thus, by comparing total *SEC*, we found out that operation at $Q_r/Q_f = 1.5$ or 2.0 consumed the least energy. However, $Q_r/Q_f = 1.5$ gave higher peak pressure: 19.9 bar compared to only 18.8 bar at $Q_r/Q_f = 2.0$. Therefore, $Q_r/Q_f = 2.0$ was preferred as the optimum operating point. Moreover, the membrane rejection slightly improved with Q_r/Q_f which may be due to lower concentration polarization at high Q_r/Q_f. Note that the average measured rejection of 0.936 is consistent with the value of 0.94 used in the modelling.

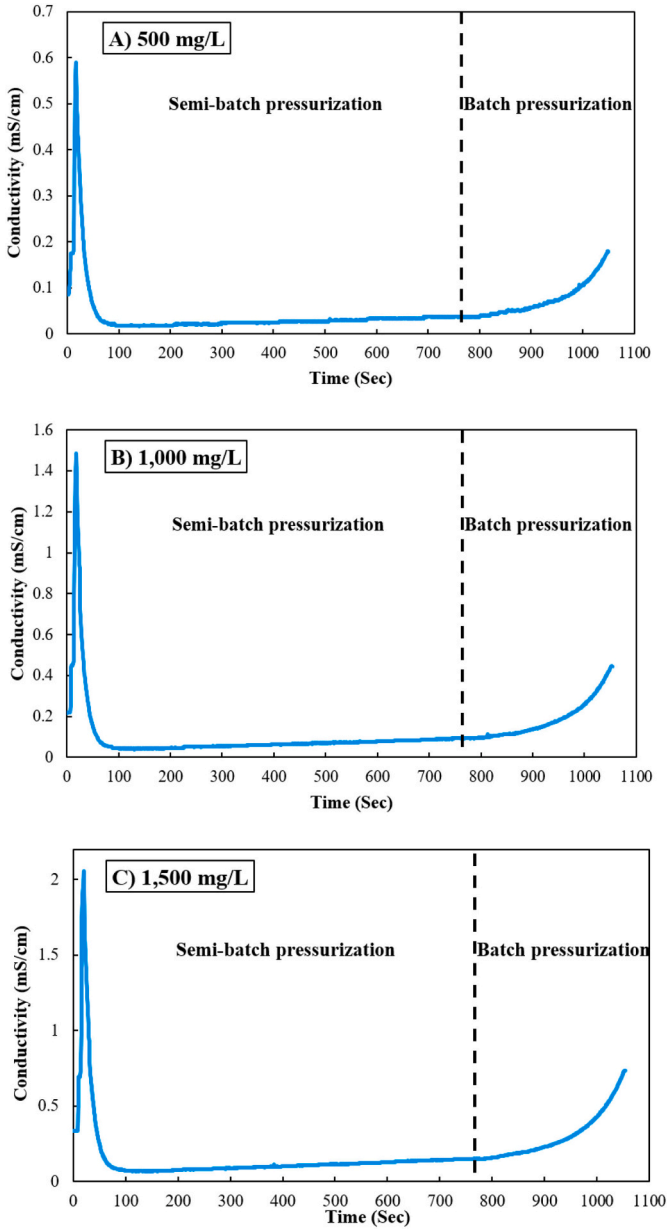

Fig. 12. Permeate conductivity vs. time over the semi-batch and batch pressurization phases at recovery $r = 0.94$, flux $J_w = 21.3$ L/m^2/h, and feed salinity A) $c_{feed} = 500$ mg/L, B) $c_{feed} = 1000$ mg/L, and C) $c_{feed} = 1500$ mg/L. See SI section 5 for conversion between conductivity and concentration.

5.7. Effect of permeate flux

Besides increasing *SEC*, permeate flux affects other parameters in the HSBRO system including rejection, peak pressure and output. We investigated a range of fluxes at $r = 0.952$, and 1000 mg/L feed salinity, to evaluate the effect on such parameters (Table 5). On increasing flux by nearly double, from 12.1 to 23.6 L/m^2/h, total pressurization *SEC* increased by 31 % (contributed mainly by the supply pump) while system output rose by 90 % from 11.56 to 21.9 m^3/day. Thus, there is a trade-off between lowered *SEC* or increased output.

Associated with this flux increase, the average pressure required during the pressurization phase increased by 46 % (from 7.07 to 10.32 bar). Alongside, peak pressure increased by 27 % (from 18.7 to 23.8 bar), and the switch pressure (from semi-batch to batch pressurization) increased by 47 % from 7.5 to 11 bar. However, semi-batch and batch pressurization duration approximately halved. Salt rejection also increased by 4 %, confirming that we can achieve higher permeate quality at high fluxes but at the expense of higher *SEC* — as in a conventional RO system.

5.8. Effect of varying switch pressure

We investigated the effect of changing the switch pressure on concentration factor, *SEC*, and peak pressure. The switch pressure determines when the system switches from semi-batch to batch pressurization. Increased switch pressure resulted in a longer semi-batch pressurization phase. These experiments were carried out at a constant flux $J_w = 16.5$ L/m^2/h and 1000 mg/L feed salinity.

5.8.1. Effect of switch pressure on concentration factor

HSBRO is a promising technology not only for water production but also for valuable component extraction from water sources. In such applications, it is desirable to concentrate maximally the feed water. Therefore, we studied the concentration factor (CF) which was calculated using Eq. (26). Fig. 15A shows the increase of CF and recovery with switch pressure. A longer semi-batch pressurization phase resulted in a higher concentration at the onset of batch pressurization and thus a higher final concentration. When switch pressure rose from 8.1 to 10.2 bar, semi-batch duration increased from 1117 to 1976 s, CF increased by 51 % from 16.3 to 24.6, and recovery increased from $r = 0.943$ to $r = 0.963$.

5.8.2. Effect of switch pressure on SEC

SEC also increased with switch pressure. Hydraulic *SEC* increased by 13 % from 0.242 to 0.274 kWh/m^3 while electrical *SEC* increased by 7 % from 0.459 to 0.491 kWh/m^3 (Fig. 15B). As explained in Section 5.3, electrical *SEC* increased less because of the higher efficiency of the supply pump at higher operating pressures.

5.8.3. Effect of switch pressure on peak pressure

Fig. 15C shows that peak pressure increased alongside CF, reaching a maximum of 24.8 bar at a switch pressure of 10.2 bar, while the average pressure was 9.14 bar. As 25 bar was the design limit of our experimental system, this peak pressure limited the CF that could be achieved. However, future systems with higher pressure ratings will enable even higher CF.

6. Discussion

6.1. Comparison with non-hybrid systems

To compare the HSBRO system against the options of non-hybrid semi-batch RO or batch RO, we used our validated model to compare the three options in achieving a recovery of 0.94 (see Table 6).

The results show that the *SEC* of the HSBRO is close to that of the batch RO, while the work exchanger volume (V_{b0}) is around four times smaller; 69 L for HSBRO compared to 265 L for batch RO. This confirms that the HSBRO option is advantageous in achieving a low *SEC* (almost as low as with batch RO) with a much more compact work exchanger. In semi-batch RO, although there is no need for a work exchanger, the *SEC* is almost 63 % higher than HSBRO and batch RO. The fourth row in Table 6 shows that a further reduction in work exchanger may also be acceptable to make the system even more compact. A reduction in V_{b0} from 69 to 40 L increases *SEC* by just 7 %.

6.2. Comparisons against existing systems

In this section, we compare our results against earlier studies with the help of second law efficiency. Second law efficiency is defined as the ratio of the minimum work of separation to the total actual work consumed in the desalination process. It illustrates how closely systems work to the reversible thermodynamic limit (a fully reversible system

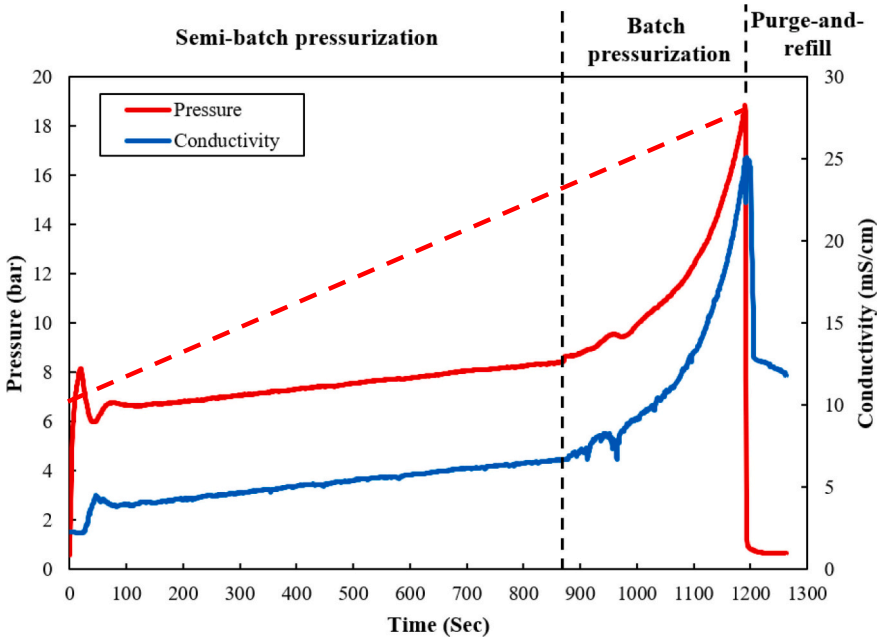

Fig. 13. Pressure and batch conductivity variations over a cycle in HSBRO system at feed salinity $c_{feed} = 1000$ mg/L ($r = 0.94$, $J_w = 18.9$ L/m^2/h). The dashed line shows the linear pressure variation that would occur in non-hybrid semi-batch mode, corresponding to a higher energy consumption. See SI section 5 for conversion between conductivity and concentration.

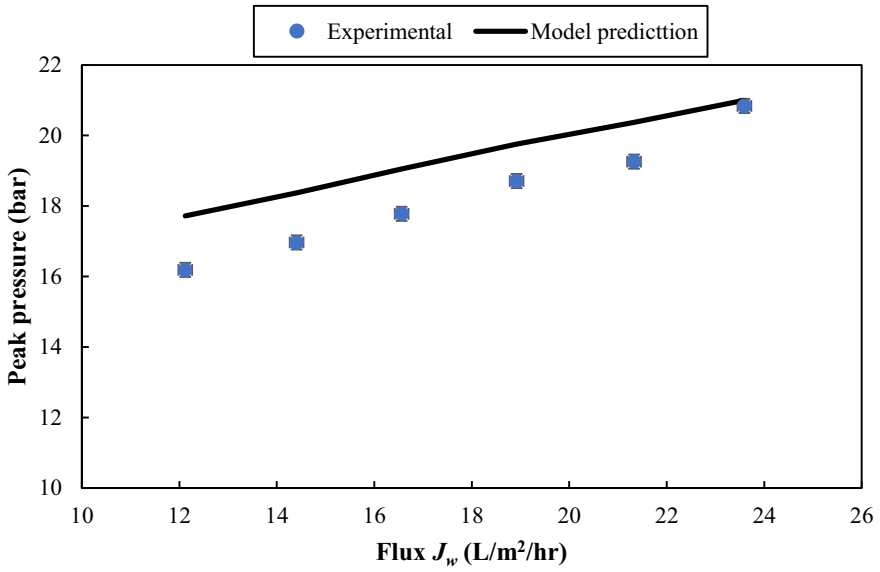

Fig. 14. Peak pressure at end of batch pressurization phase vs. water flux. Model predictions and experimental values at feed salinity $c_{feed} = 1000$ mg/L and recovery $r = 0.94$.

Table 4
Effect of varying recirculation flow rate ratio (Q_r/Q_f) on the pressurization *SEC* breakdown (by pump) and on rejection, peak pressure, and average pressure over a cycle at 1000 mg/L feed salinity, $r = 0.94$, and $J_w = 18.9$ L/m^2/h. *SEC* includes energy consumed in both semi-batch and batch pressurization phases (but not purge-and-refill phase).

Recirc. flow/feed flow Q_r/Q_f	Average pressure (bar)	Start batch pressure (bar)	Peak pressure (bar)	Rejection R_s	Electrical *SEC* over two pressurization phases (kWh/m^3)		
					Supply pump	Recirculation pump	Total
1.5	9.08	9.3	19.9	0.926	0.441	0.027	0.468
2.0	8.54	8.7	18.8	0.936	0.425	0.043	0.468
2.6	8.37	8.6	18.7	0.94	0.42	0.067	0.487
3.2	8.28	8.6	18.7	0.942	0.416	0.103	0.519
3.7	8.23	8.5	18.7	0.943	0.415	0.151	0.566

Table 5
Effect of varying flux on measured parameters of HSBRO system at 1000 mg/L feed salinity and recovery $r = 0.952$. System flux averaged over the whole cycle, including the purge-and refill phase which is non-productive.

Flux during press. J_w (L/m^2/h)	System flux (L/m^2/h)	Semi-batch duration (s)	Batch duration (s)	Purge-and-refill duration (s)	Transition pressure semi-batch to batch (bar)	Average pressure during pressurization phase (bar)	Rejection R_s	Output (m^3/day)	Peak pressure $\widehat{P}$ (bar)	Electrical *SEC* over two pressurization phases (kWh/m^3)		
										Supply pump	Recirculation pump	Total
12.1	11.7	1858	504	77	7.5	7.07	0.9	11.56	18.7	0.38	0.035	0.415
14.4	13.9	1559	424	77	8.2	7.70	0.91	13.65	19.7	0.398	0.035	0.433
16.6	15.9	1358	367	77	8.8	8.28	0.919	15.62	20.6	0.417	0.039	0.456
18.9	18.0	1191	322	77	9.5	8.95	0.925	17.74	21.5	0.441	0.044	0.485
21.3	20.2	1059	286	77	10.2	9.63	0.931	19.87	22.5	0.465	0.049	0.514
23.6	22.3	946	257	76	11.0	10.32	0.936	21.91	23.8	0.49	0.055	0.544

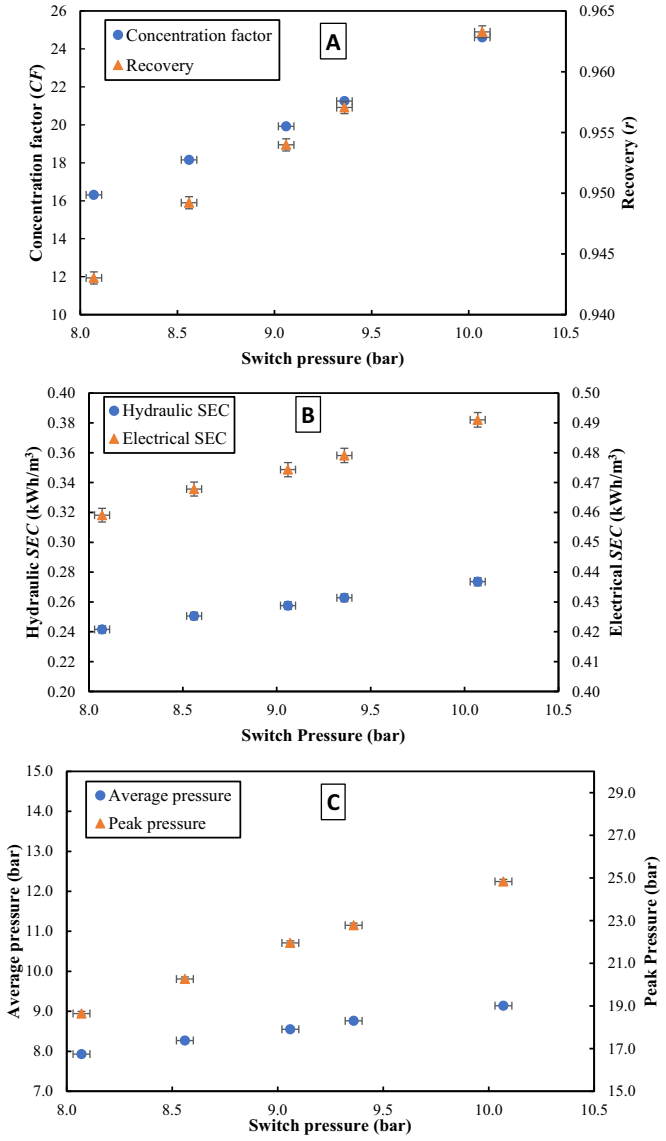

Fig. 15. Effect of varying switch pressure on: A) concentration factor (CF) and recovery (r), B) hydraulic and electrical *SEC*, C) average and peak pressure. Feed salinity 1000 mg/L and $J_w = 16.5$ L/m^2/h.

has a second law efficiency of 100 %) and can help identify potential for improvement. We use second law efficiency to make a fair comparison against other studies, taking into account variations in recovery and feed concentration.

To ensure a fair comparison, we have applied certain criteria in selecting those studies against which to compare. Firstly, the systems should be high recovery. At recovery below about 70 %, the HSBRO system is probably not needed; a non-hybrid batch RO system would be adequate, as described previously [44]. Secondly, we have selected systems using brackish feed, rather than seawater feed, as seawater systems typically provide a significantly higher 2nd law efficiency [65] such that direct comparison with brackish water systems could be misleading. In addition, seawater systems rarely achieve recovery above 70 %. Thirdly, we have selected only experimental (not theoretical) studies, in which the systems have been piloted at least at laboratory scale. Fourthly, the systems selected are ones where second law efficiency is reported, or where sufficient information is given for second law efficiency to be calculated. The studies selected are mostly multi-stage RO systems, or batch or semi-batch RO systems.

Table 6
Comparison of HSBRO against non-hybrid options ($r = 0.94$, $J_w = 18.9$ L/m^2/h, feed concentration of 1000 mg/L, 60 % pump efficiencies assumed throughout all three phases; 8-inch Eco Pro-440 membrane used as in this study).

Option	Hydraulic *SEC* (kWh/m^3)	Electrical *SEC* (kWh/m^3)	Work exchanger volume V_{bo} (L)	Notes
Semi-batch RO	0.415	0.692	0	
Batch RO	0.254	0.423	265.0	
HSBRO	0.255	0.425	69.0	Current study
HSBRO	0.273	0.455	40.0	Reduced work exchanger volume

Although batch RO is theoretically the most efficient configuration in RO systems, comparison of HSBRO and batch RO at 1000 mg/L showed that second law efficiency of HSBRO is actually slightly higher than batch RO: 13.1 % (see Table 6) against 9.2 % (calculated using Eq. 25 and data in [44]). Electrical *SEC* for both systems were nearly the same around 0.49 kWh/m^3, even though the HSBRO achieves much higher recovery. This finding is consistent with [15] and explained by reduction in minor losses in the refill stage of HSBRO. The SEC_{ideal} of HSBRO is slightly larger than for batch RO, because of the higher recovery, resulting in improved second law efficiency.

Semi-batch RO (or closed-circuit RO) is another configuration that has attracted much attention over the last decade. Efraty et al. [17] reported electrical *SEC* of 0.77 kWh/m^3 for two cases using semi-batch RO. In the first case, the feed conductivity was 6.8 mS/cm, recovery r was 0.8, flux $J_w = 19$ L/m^2/h, the high-pressure pump efficiency was 55 %, and rejection of 90.8 % was achieved. In the second case, feed conductivity was 4.0 mS/cm, recovery r was 0.88, flux J_w was 27 L/m^2/h, the high-pressure pump efficiency was 60 %, and rejection of the system was 88 %. Since the authors did not mention the feed analysis, by assuming that the feed source is like a NaCl solution, we calculated the osmotic pressure and then second law efficiency. The latter had values of

20.5 and 13.6 % for the first and second cases respectively. Considering the same feed salinity, fluxes, and pump efficiencies as cases 1 and 2 but at a higher recovery of $r = 0.94$ in HSBRO, we predict electrical *SEC* of 0.93 and 0.69 kWh/m^3 for these two cases in the HSBRO system. These values correspond to second law efficiencies of approximately 24.4 and 18.4 % respectively — as such considerably better than the values of 20.5 and 13.6 % mentioned above for semi-batch RO. Additionally, considering the same recovery as cases 1 and 2, we predict electrical *SEC* of 0.69 and 0.49 kWh/m^3 in the HSBRO system respectively. Corresponding second law efficiency values were 22.9 and 21.3 %.

Kahraman et al. [54] reported second law efficiency of 8 % for a two-stage brackish RO plant at a feed concentration of 900 mg/L and recovery $r = 0.72$. However, using their data and Eq. (25), second law efficiency was calculated 3.8 % which is around three times lower than the value of 13.1 % for the HSBRO system at 1000 mg/L feed salinity. Second law efficiency of only 4.1 % was reported for a two-stage RO plant in Jordan using actual plant data [59]. This plant was fed with brackish water of 2450 mg/L salinity (electrical conductivity of 3.95 mS/cm) and a combined pump-motor efficiency of 75 % was used in the calculations. In another case study, Sharqawy et al. [66] analysed the performance of a RO plant in California (USA) fed with underground brackish water at a salinity of about 1550 mg/L. The value reported for the second law efficiency was 1.51 % considering pump efficiency of 100 %. At similar feed salinity in the HSBRO system, we achieved second law efficiency of 17.8 %. It is also interesting that they calculated how much second law efficiency would increase by adding an energy recovery device; the predicted increase was marginal from 1.51 to 1.73 %. More recently, a medium-sized two-stage brackish RO plant of the Arab Potash Company with $r = 0.68$ was analysed. This plant was fed with brackish water with a salinity of 1098.6 mg/L and second law efficiency of 4.48 % was reported for the whole RO plant [67].

We also believe that HSBRO can improve second law efficiency for more saline feeds including seawater. This will be evaluated in future studies.

6.3. Potential improvements

In this section, we use our validated model to assess the benefits of future improvements to the HSBRO system.

6.3.1. Effect of membrane water permeability on hydraulic SEC

Thanks to advances in membrane material and manufacturing technology, the water permeability of RO membranes has gradually improved over the last few decades, while high salt rejection has been maintained [68]. We expect this trend to continue. Therefore, we have predicted the effect of improved water permeability on hydraulic *SEC* (see Fig. 16). We assumed 1000 mg/L feed concentration, $J_w = 18.9$ L/m^2/h, and $r = 0.94$. We project that, by increasing membrane water permeability from 3 to 6 and 9 L/m^2/h/bar, the hydraulic *SEC* will decrease by 29.1 and 39.0 % respectively (from 0.313 to 0.222 and 0.191 kWh/m^3). The membrane element used in this study (Eco Pro-440) had a water permeability of $A_w = 4.4$ L/m^2/h/bar, as measured experimentally using RO permeate water and confirmed throughout this study.

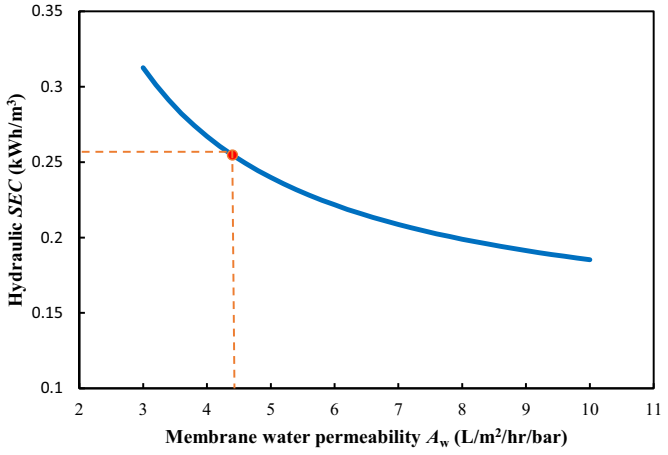

Fig. 16. Predicted hydraulic *SEC* as a function of membrane water permeability (*A* value) at 1000 mg/L feed concentration, $r = 0.94$, and $J_w = 18.9$ L/m^2/h. The orange point indicates the experimental value for the Eco Pro-440 membrane used in this study.

6.3.2. Effect of valve size on hydraulic SEC

Fig. 17 shows the effect of valve orifice diameter on hydraulic *SEC* in the HSBRO system. The model predicted how hydraulic *SEC* will change with valve size at 1000 mg/L feed concentration, $J_w = 18.9$ L/m^2/h, and $r = 0.94$. On increasing the valve orifice diameter from 15 (current study) to 20 and 25 mm, hydraulic *SEC* will reduce by 5.4 and 6.9 %. This energy saving results from a reduction in friction losses [44].

6.3.3. Effect of pump efficiency on hydraulic SEC

As discussed in Section 5.3, pump efficiencies have a considerable impact on the total electrical energy consumed by the HSBRO system. More efficient pumps will lower electrical *SEC*, making the HSBRO system even more attractive for various industries and applications. Fig. 18 compares electrical *SEC* of the current HSBRO against some hypothetical cases (assuming the same efficiency for both pumps during all three operation phases) at different feed salinities, $J_w = 18.9$ L/m^2/h, and $r = 0.94$. As can be seen, with pump efficiency uniformly improved to 60 %, electrical *SEC* would decrease by 20, 12.7, and 4.3 % at 500, 1000, and 1500 mg/L feed concentrations respectively. However, by implementing pumps with 80 % efficiency, electrical *SEC* would reduce by 40 % (from 0.42 to 0.252 kWh/m^3), 34.7 % (from 0.487 to 0.318 kWh/m^3), and 28.4 % (from 0.536 to 0.384 kWh/m^3) at 500, 1000, and 1500 mg/L respectively.

6.3.4. Combined improvements

To reduce overall *SEC* further, the above improvements of high-permeability membranes, more efficient pumps, and bigger valve size can be combined for the best overall performance. Accordingly, we modelled the overall electrical *SEC* of the HSBRO system assuming membranes with a permeability of $A_w = 10$ L/m^2/h/bar, valve orifice diameter of 25 mm, and 80 % efficiency for both pumps. Table 7 shows the predicted results at different feed salinities, with $J_w = 18.9$ L/m^2/h, and $r = 0.94$. These predictions are also compared with the ideal system

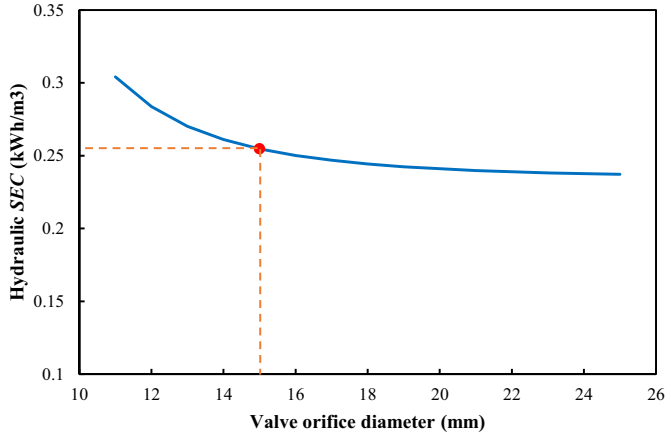

Fig. 17. Model predictions of hydraulic SEC as a function of valve diameter in the HSBRO system at 1000 mg/L feed concentration, $J_w = 18.9$ L/m^2/h, and $r = 0.94$. The orange point is the valve diameter used in the current prototype.

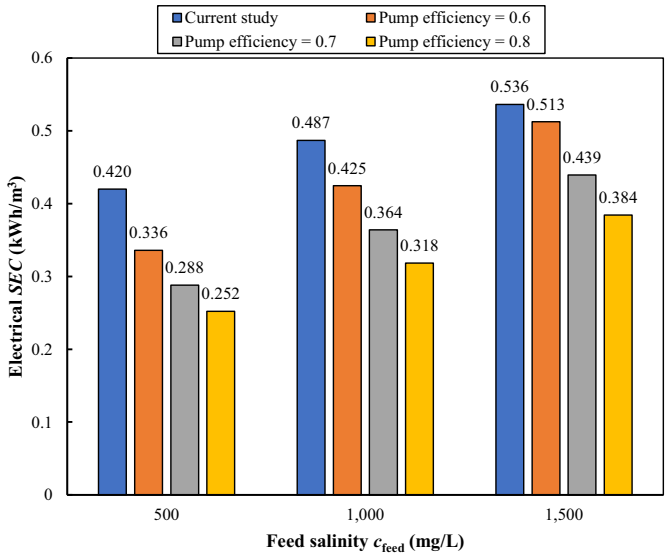

Fig. 18. Projection of electrical *SEC* according to pump efficiencies at various feed salinities, $J_w = 18.9$ L/m^2/h, and $r = 0.94$.

Table 7
Theoretical ideal minimum *SEC* compared to the experimental results for the current HSBRO system, and to predicted electrical *SEC* after improvements in membrane water permeability ($A_w = 10$ L/m^2/h/bar), pump efficiencies (80 % for both supply and recirculation pumps) and valve orifice diameter (25 mm) at various feed salinities, $J_w = 18.9$ L/m^2/h, and $r = 0.94$. The corresponding second law efficiency (SEC_{ideal}/SEC) is also shown.

Feed salinity c_{feed} mg/L	Ideal system	Current HSBRO system		Model predictions after improvements	
	SEC_{ideal} (kWh/m^3)	Electrical *SEC* (kWh/m^3)	Second law efficiency (%)	Electrical *SEC* (kWh/m^3)	Second law efficiency (%)
500	0.0325	0.420	7.8	0.143	22.8
1000	0.0640	0.487	13.1	0.210	30.5
1500	0.0953	0.536	17.8	0.276	34.5

(calculated by Eq. 25) and the experimental measurements for the current system. Furthermore, Table 7 shows second law efficiency (SEC_{ideal}/SEC) for general comparison against existing RO plants.

With all three improvements implemented, electrical *SEC* of the HSBRO system would decrease by 66.0 %, 56.9 %, and 48.5 % at 500, 1000, and 1500 mg/L feed concentrations respectively. This corresponds to a considerable electrical *SEC* decrease from the range of 0.42–0.536 to that of 0.143–0.276 kWh/m^3 at 500–1500 mg/L feed concentration. Nevertheless, the predicted *SEC* after improvements remains higher than SEC_{ideal}, showing that there is still room for improvement.

6.4. Operation at higher salinities

Today's RO systems are limited to about 120 bar, as determined by the maximum allowable pressure specified by membrane manufacturers. Therefore, peak pressure is an important consideration if the HSBRO system is to operate at high recovery, such as $r = 0.95$, and at high feed salinity. The Eco Pro-440 module used for treating brackish water in this study is limited to 41 bar. Using this membrane specification in our experimentally validated model, we predicted the performance of the HSBRO system up to 4000 mg/L feed concentration at two recoveries, $r = 0.90$ and 0.95 (see Table 8). Electrical *SEC* was calculated assuming 60 % pump efficiency for both pumps. Additionally, for higher concentrations, we applied XUS180808 module specifications i.e. membrane area of 30.6 m^2 and permeability of $A_w = 1.39$ L/m^2/h/bar based on the manufacturer's datasheet. This module can withstand pressures up to 120 bar.

Using the Eco Pro-440 module, HSBRO can desalinate feed sources up to around 4000 mg/L at $r \geq 0.9$ and $J_w = 18.9$ L/m^2/h, while staying within the peak pressure limitation of 41 bar. Although peak pressure seems to be a major limitation for HSBRO, in all cases presented in Table 8 for this module, average pressure during semi-batch and batch phases will not exceed 11.7 and 21 bar respectively, meaning that the operating pressure is lower than the 41 bar limit during most of the cycle. Operation at pressures near the limit occur only during the last seconds of the batch pressurization phase and last for a short period of time (<3 % of process time). Thus, we do not expect that the module would be damaged since this limitation applies to continuous operation normally. Nonetheless, by reducing the duration of semi-batch pressurization (resulting in lower recovery), we can decrease the peak pressure and eliminate this risk. For example, at 3000 mg/L feed concentration, although the average batch pressure is 29.1 bar, the peak pressure reaches 60 bar, clearly exceeding the 41 bar limit. Therefore, by reducing the recovery to $r = 0.923$, we predict that the peak pressure will decrease to 40.7 bar, which is within the limit for the Eco Pro-440 module.

Regarding *SEC* using the Eco Pro-440 module, hydraulic *SEC* ranges from 0.268 to 0.431 kWh/m^3 and electrical *SEC* ranges from 0.446 to 0.718 kWh/m^3 at 1000–3000 mg/L feed salinity, with $J_w = 18.9$ L/m^2/h, and $r = 0.95$ (except at 3000 mg/L feed solution where recovery is reduced to $r = 0.923$). However, at $r = 0.9$, these values decrease to 0.234–0.398 kWh/m^3 for the hydraulic *SEC*, and 0.391–0.663 kWh/m^3 for electrical *SEC*. Maximum achievable recovery at 4000 mg/L (observing the pressure limit) is $r = 0.9$ and gives hydraulic and electrical *SEC* of 0.48 and 0.799 kWh/m^3, respectively. Additionally, for this module at $r \geq 0.9$ and $R_s = 0.94$, we predict second law efficiency ranging from 14.2 % at 1000 mg/L to 27.8 % at 4000 mg/L — a substantial improvement on earlier studies mentioned in Section 6.2.

We also predict that the HSBRO system using an ultra-high pressure XUS180808 module can treat water sources with salinity up to 10,000 mg/L while operating at recoveries higher than $r \geq 0.9$, at flux $J_w = 18.9$ L/m^2/h, without exceeding the pressure limit of 120 bar. For instance, when operating at $r = 0.9$, peak pressure varies from 57 to 115 bar at feed salinities ranging from 4000 to 10,000 mg/L while semi-batch and batch average pressure is in the range of 30–37 and 35–60 bar, respectively. Hydraulic *SEC* is in the range of 0.9–1.41 kWh/m^3 while electrical *SEC* is 1.5–2.35 kWh/m^3. Furthermore, second law efficiency ranges from 14.8 to 23.7 %. Such high feed salinity and high recovery is important for ZLD applications.

Comparing the two membranes at $r = 0.9$ and 4000 mg/L feed salinity, the hydraulic *SEC* of the XUS180808 module is almost twice that of the Eco Pro-440 module; 0.9 against 0.48 kWh/m^3. The main reason for this increase is the lower permeability of the XUS180808 compared to the Eco Pro-440 membrane. Future work will include verifying the performance with the XUS180808 or similar membranes, noting that there are several practical challenges to address in implementing such high-pressure RO systems [69].

Fig. 19 gives an overall summary of the above findings regarding second law efficiency of the HSBRO and other comparable systems. For HSBRO, it shows experimental values and those predicted after improvements to the system. It also includes model predictions at higher feed salinities using two different RO modules. For comparison, Fig. 19 further includes experimental results from batch RO and other experimental studies in high-recovery RO. Second law efficiency in HSBRO and batch RO generally increases with feed salinity. At similar salinity, HSBRO gave the highest second law efficiency compared to other studies (even batch RO) and this can be increased further by implementing some improvements such as more efficient pumps and high permeability membranes.

Table 8
Prediction of hydraulic and electrical *SEC* (assuming 60 % pump efficiency for both pumps), peak and average pressure for the HSBRO system at a wide range of feed salinities, $J_w = 18.9$ L/m^2/h, and two different recoveries. The prediction is based on the properties of the Eco Pro-440 membrane (41 bar limit) and the ultra-high pressure XUS180808 membrane (120 bar limit). Second law efficiency was calculated assuming rejection of $R_s = 0.94$. The italicized values (marked not applicable, NA) of peak pressure show where the limit is exceeded and therefore recovery must be decreased to lower the peak pressure. Recoveries corresponding to operation near the pressure threshold are marked *.

Membrane type	Feed salinity (mg/L)	Recovery	Hydraulic *SEC* (kWh/m^3)	Electrical *SEC* (kWh/m^3)	Peak pressure (bar)	Average semi-batch pressure (bar)	Average batch pressure (bar)	Second law efficiency (%)
BW Eco Pro-440	1000	0.95	0.268	0.446	23.1	7.6	12.8	15.2
		0.9	0.234	0.391	13.9	6.2	8.7	14.2
	2000	0.95	0.390	0.649	41.6	10.9	20.9	20.9
		0.9	0.316	0.527	23.2	8.1	12.8	21.1
	3000	0.95 (*NA*)	0.512 (*NA*)	0.853 (*NA*)	*60* (*NA*)	14.2 (*NA*)	29.1 (*NA*)	(*NA*)
		0.923*	0.431	0.718	40.7	11.2	20.5	25.1
		0.9	0.398	0.663	32.4	9.9	16.9	25.2
	4000	0.95 (*NA*)	0.633 (*NA*)	1.056 (*NA*)	*78.6* (*NA*)	17.4 (*NA*)	37.3 (*NA*)	(*NA*)
		0.9	0.480	0.799	41.5	11.7	21	27.8
XUS 180808 (ultra-high pressure)	4000	0.95	1.043	1.738	95.1	31.5	51.3	15.6
		0.9	0.900	1.501	57.4	25.9	35.2	14.8
	5000	0.95	1.167	1.945	114.2	34.7	59.4	17.4
		0.9	0.985	1.642	67	27.7	39.3	16.9
	6000	0.95 (*NA*)	1.291 (*NA*)	2.152 (*NA*)	*133.3* (*NA*)	37.9 (*NA*)	67.6 (*NA*)	(*NA*)
		0.94*	1.217	2.028	114.8	35.2	59.7	19.1
		0.9	1.070	1.783	76.7	29.6	43.4	18.7
	7000	0.95	NA	NA	NA	NA	NA	NA
		0.93*	1.264	2.107	114.6	35.5	59.6	20.5
		0.9	1.155	1.925	86.4	31.4	47.6	20.2
	8000	0.95	NA	NA	NA	NA	NA	NA
		0.92*	1.316	2.193	115.7	36.1	60	21.7
		0.9	1.240	2.067	96.1	33.2	51.7	21.5
	9000	0.95	NA	NA	NA	NA	NA	NA
		0.91*	1.362	2.270	115.3	36.5	59.9	22.8
		0.9	1.325	2.208	105.7	35.1	55.8	22.7
	10,000	0.95	NA	NA	NA	NA	NA	NA
		0.9	1.410	2.350	115.4	36.9	60	23.7

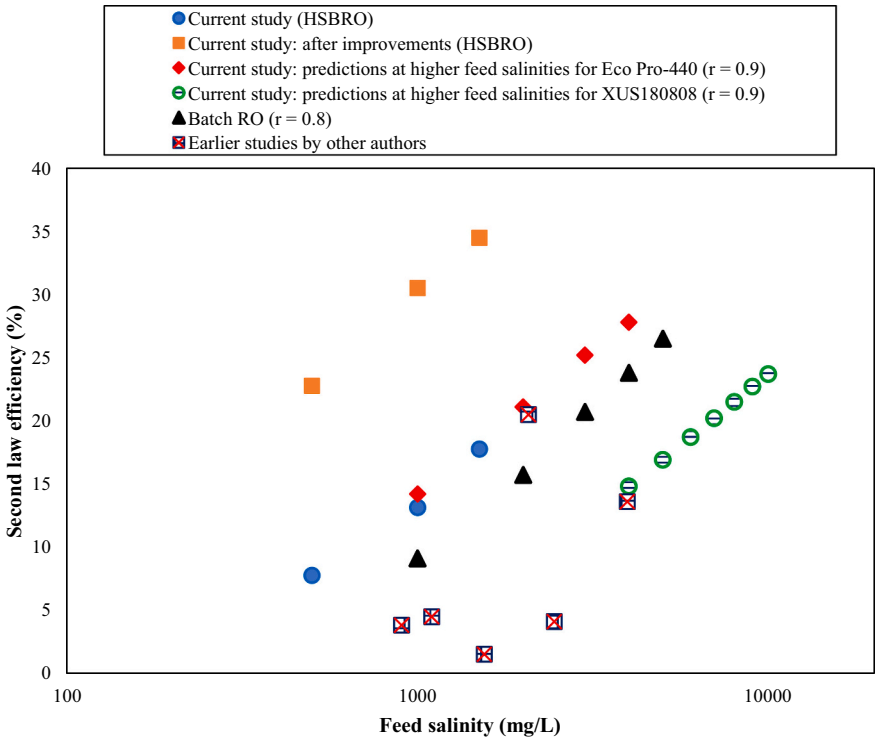

Fig. 19. Comparison of second law efficiency in the current study against batch RO and other earlier experimental RO studies, as a function of feed salinity.

6.5. Further improvements and future research

Future developments of the HSBRO system could also include modifications at the brine outlet to retard the pressure surge at the beginning of the purge-and-refill phase. It is possible that such an arrangement could reduce the amount of osmotic backflow and recover a small amount of energy. Based on an initial estimate of the hydraulic energy contained in the pressure surge, the potential for energy recovery is limited to about 2 % of overall SEC but may be worth considering for future optimization.

Another development may concern the design of the supply pump arrangement. As seen in Table 3 above, the efficiency of the supply pump dropped from about 60 % to only ~10 % during purge and refill. This is because the supply pump is a positive displacement pump that is not optimized to run at low pressure. A centrifugal pump would likely achieve efficiency >50 %, thus substantially reducing the electrical *SEC* contribution during purge and refill, which currently accounts for about 1–5 % of total *SEC*. Therefore, it may be beneficial to use a combination of a positive displacement pump (for pressurization) and a centrifugal pump (for purge and refill) — albeit at the cost of added complexity.

In future research, the inherent advantages and energy losses of HSBRO may further be investigated based on theoretical analyses. It would be valuable to carry out a complete exergy analysis (in comparison to multi-stage RO, semi-batch RO, and advanced system designs such as EERO) and to present the results with the help of Sankey and Grassman diagrams.

7. Conclusions

For the first time in RO studies, we experimentally investigated the performance of a hybrid semi-batch/batch RO (HSBRO) system. Using a single-acting free-piston design and an 8-inch RO module (Eco Pro-440), HSBRO achieves an output of 15–22 m^3/day at recovery of 0.94. The HSRBO is no more complex than batch RO, requiring only a modification to the controller program to alter the sequence of valve operation. The main conclusions are:

- Operating at flux J_w = 18.9 L/m^2/h, recovery r = 0.94, and feed concentrations c_{feed} of 500 to 1500 mg/L, HSBRO gives hydraulic and electrical *SEC* in the range of 0.2–0.31 and 0.42–0.54 kWh/m^3 respectively, with an output of 17.5 m^3/day, and salt rejection of R_S = 93–94 %.
- The greatest component of energy consumption comes from the supply pump during the pressurization phases, which contributes 86–89 % of the total *SEC*; whereas the recirculation pump contributes only 10–12 % over the whole cycle. Optimum recirculation flow (at the RO module brine outlet) to the feed pump flow is around 2; at higher flow ratios, the total *SEC* increases substantially (although slightly higher salt rejection is achieved).
- An updated and validated model gives *SEC* agreement of 1–3 % with experiment, using explicit algebraic equations thus avoiding the need for numerical algorithms. Two important adjustable parameters were used in the model: membrane permeability and system salt rejection.
- When the system reaches a stable condition, salt retention between cycles causes the initial concentration to be around 89 % higher than the feed concentration, increasing the applied pressure and energy consumption. This can be reduced to 44 % by purging for longer, thus saving 7 % in electrical *SEC* (but at the expense of system recovery falling from 94 to 91.3 %). The updated model accurately represents salt retention, taking into account both salt rejection and osmotic backflow.
- Due to salt diffusion during the purge-and-refill phase, there is an initial peak in the permeate quality which has a negative effect on salt rejection, causing a 0.6–0.9 % decrease in the total rejection of the system.
- A concentration factor of 24.6 and recovery r = 0.96 are achieved at feed salinity c_{feed} = 1000 mg/L with electrical *SEC* < 0.5 kWh/m^3, making HSBRO an attractive option that can be implemented in many industries particularly for extraction of valuable components from effluents. Using ultra high-pressure RO membranes that have recently become available, we will be able to achieve even higher concentration factors.
- Compared to semi-batch RO under similar conditions, HSBRO consumes 63 % less energy. Compared to batch RO, although HSBRO energy consumption is almost the same, the HSBRO work exchanger size is almost four times smaller at recovery r = 0.94. HSBRO can achieve recovery up to r = 0.98 at low feed salinities, just by operating for longer in semi-batch mode.
- Second law efficiency is in the range of 7.8–17.8 % for feed concentrations of 500–1500 mg/L. The second law efficiencies measured equal or exceed those for other high-recovery experimental systems reported in the literature (not only multi-stage RO systems but also the batch and semi-batch RO).
- The validated model enables us to predict the effect of improvements, such as using high-permeability membranes and more efficient pumps, to lower electrical *SEC* to 0.14–0.28 kWh/m^3 and improve second law efficiency up to 34.5 % for feed salinities of c_{feed} = 500–1500 mg/L.
- With ultrahigh-pressure RO membranes, the model predicts that feed solutions with concentration c_{feed} = 10,000 mg/L can be treated, with recovery $r \geq 0.9$, hydraulic *SEC* < 1.4 kWh/m^3 and second law efficiency up to 23.7 %.

The hybrid concept allows energy efficiency close to that of batch RO, even at very high recoveries $r \geq 0.94$, in a much more compact arrangement. Nonetheless, there are still challenges in scaling this solution to larger systems with output greater than about 100 m^3/day. Therefore, future work should focus on this scale up challenge. There is also a need for experimental work at higher pressures to validate the predictions for highly concentrated feed and brine solutions, as needed for ZLD and MLD applications. This should include studies of organic and inorganic fouling using substances encountered in such applications.

Nomenclature

Roman and Greek symbols

A_w	L/m^2/h/bar, water membrane permeability
A_m	m^2, membrane area
c	mg/L, concentration
$\bar{c}$	mg/L, average of initial and final concentration
c_0	mg/L, initial concentration of semi-batch phase
c_1	mg/L, initial concentration of batch phase
c_{feed}	mg/L, feed concentration
c_{max}	mg/L, initial concentration leaving the system at the start of the purge phase
$c_{permeate}$	mg/L, permeate concentration
C_d	-, coefficient of discharge
E	kJ (kWh), energy consumption
E_{P1}	kJ (kWh), energy consumption of semi-batch pressurization phase
E_{P2}	kJ (kWh), energy consumption of batch pressurization phase
$E_{P\&R}$	kJ (kWh), energy consumption of purge-and-refill phase
J_w	m/s (L/m^2/h), permeate flux
P	kPa (bar), pressure
$\overline{P}$	kPa (bar), volume-weighted average pressure
$\overline{P_1}$	kPa (bar), volume-weighted average pressure during semi-batch phase
$\overline{P_2}$	kPa (bar), volume-weighted average pressure during batch

	phase
$\widehat{P}$	kPa (bar), maximum peak pressure
Q	m^3/s, flow rate
Q_f	m^3/s, feed flow rate
Q_r	m^3/s, recirculation flow rate
R_s	–, salt rejection
r	–, recovery
r_b	–, recovery in batch phase
r_p	–, recovery in pressurization phase
r_{sb}	–, recovery in semi-batch phase
S_{L1}	–, longitudinal concentration gradient factor during semi-batch phase
S_{L2}	–, longitudinal concentration gradient factor during batch phase
S_P	–, concentration polarization factor
S_R	–, salt retention factor
V	m^3, volume
V_0	m^3, initial volume of the system
V_{b0}	m^3, work exchanger swept volume
V_{back}	m^3, backflow volume
V_{brine}	m^3, brine volume
V_{feed}	m^3, feed volume
$V_{permeate}$	m^3, permeate volume
V_{pg}	m^3, nominal purge volume
$V_{pipe,R}$	m^3, retained solution volume in pipes
V_{sb}	m^3 volume supplied during the semi-batch phase
ΔP	kPa, pressure drop
ΔP_m	kPa, cross-flow pressure drop in the RO module
ΔP_s	kPa, piston seal pressure drop
ΔP_v	kPa, valve pressure drop
ΔP_{v1}	kPa, bypass valve pressure drop
ΔP_{v2}	kPa, recirculation valve pressure drop
ΔP_{v3}	kPa, brine valve pressure drop
Π_{feed}	kPa, feed osmotic pressure
λ	–, longitudinal dispersion parameter

Abbreviations

CF	concentration factor
COMRO	cascading osmotically mediated reverse osmosis
CRO	centrifugal reverse osmosis
CT	conductivity transmitter
EERO	energy efficient reverse osmosis
ERD	energy recovery device
EXP	experimental
FT	flow transmitter
HPRO	high pressure reverse osmosis
HSBRO	hybrid semi-batch/batch reverse osmosis
LSRRO	low salt rejection reverse osmosis
MLD	minimum liquid discharge
MOD	model
MVC	mechanical vapour compression
OARO	osmotically assisted reverse osmosis
P	pressurization
PFD	plug flow desalination
P&R	purge-and-refill
PT	pressure transmitter
RO	reverse osmosis
FO	forward osmosis
UF	ultrafiltration
RP	recirculation pump
SEC	specific energy consumption
SI	supporting information
W1	weighing platform (feed tank)
W2	weighing platform (permeate tank)
W3	weighing platform (brine tank)
ZLD	zero liquid discharge

CRediT authorship contribution statement

EH: Writing - original draft, Experimental investigation.
SK: Background investigation, Writing – review & editing.
SB: Review & editing, Background investigation.
KP: Review & editing, Background investigation.
PD: Conceptualization, Theory, Writing – review & editing, Supervision, Project administration, Funding acquisition.

Declaration of competing interest

The authors would like to declare that a spinout company has been formed to exploit the technology described in this article, and that two of the authors (KP and PAD) have an equity stake in the spinout company.

Data availability

Experimental data files are included in the Supplementary material.

Acknowledgements

This project has received funding from the European Union's Horizon 2020 research and innovation programme under grant agreements No 820906 and No 958454, and from the National Research Foundation of Korea (NRF) grant funded by the Korean government (MSIT) (No. NRF-2021R1F1A1055769).

Appendix A. Supplementary data

Supplementary data to this article can be found online at https://doi.org/10.1016/j.desal.2022.116126.

References

[1] M. Elimelech, A.Phillip William, The future of seawater desalination: energy, technology, and the environment, Science 333 (2011) 712–717.
[2] P.S. Goh, H.S. Kang, A.F. Ismail, N. Hilal, The hybridization of thermally-driven desalination processes: the state-of-the-art and opportunities, Desalination 506 (2021), 115002.
[3] K. Park, J. Kim, D.R. Yang, S. Hong, Towards a low-energy seawater reverse osmosis desalination plant: a review and theoretical analysis for future directions, J. Membr. Sci. 595 (2020), 117607.
[4] E. Jones, M. Qadir, M.T.H. van Vliet, V. Smakhtin, S.-M. Kang, The state of desalination and brine production: a global outlook, Sci. Total Environ. 657 (2019) 1343–1356.
[5] J. Kim, K. Park, D.R. Yang, S. Hong, A comprehensive review of energy consumption of seawater reverse osmosis desalination plants, Appl. Energy 254 (2019), 113652.
[6] N.C. Darre, G.S. Toor, Desalination of water: a review, Curr. Pollut. Rep. 4 (2018) 104–111.
[7] A. Garciadiego, T. Luo, A.W. Dowling, Molecular design targets and optimization of low-temperature thermal desalination systems, Desalination 504 (2021), 114941.
[8] B. Sutariya, H. Raval, Analytical study of optimum operating conditions in semi-batch closed-circuit reverse osmosis (CCRO), Sep. Purif. Technol. 264 (2021), 118421.
[9] D.M. Warsinger, E.W. Tow, K.G. Nayar, L.A. Maswadeh, J.H. Lienhard V, Energy efficiency of batch and semi-batch (CCRO) reverse osmosis desalination, Water Res. 106 (2016) 272–282.
[10] A. Yusuf, A. Sodiq, A. Giwa, J. Eke, O. Pikuda, G. De Luca, J.L. Di Salvo, S. Chakraborty, A review of emerging trends in membrane science and technology for sustainable water treatment, J. Clean. Prod. 266 (2020), 121867.
[11] M.T. Mito, X. Ma, H. Albuflasa, P.A. Davies, Reverse osmosis (RO) membrane desalination driven by wind and solar photovoltaic (PV) energy: state of the art and challenges for large-scale implementation, Renew. Sust. Energ. Rev. 112 (2019) 669–685.
[12] R.H. Hailemariam, Y.C. Woo, M.M. Damtie, B.C. Kim, K.-D. Park, J.-S. Choi, Reverse osmosis membrane fabrication and modification technologies and future trends: a review, Adv. Colloid Interf. Sci. 276 (2020), 102100.
[13] J.R. Werber, A. Deshmukh, M. Elimelech, Can batch or semi-batch processes save energy in reverse-osmosis desalination? Desalination 402 (2017) 109–122.

[14] T. Tong, M. Elimelech, The global rise of zero liquid discharge for wastewater management: drivers, technologies, and future directions, Environ. Sci. Technol. 50 (2016) 6846–6855.
[15] K. Park, P.A. Davies, A compact hybrid batch/semi-batch reverse osmosis (HBSRO) system for high-recovery, low-energy desalination, Desalination 504 (2021), 114976.
[16] R.Y. Ning, T.L. Troyer, Tandom reverse osmosis process for zero-liquid discharge, Desalination 237 (2009) 238–242.
[17] A. Efraty, Closed circuit desalination series no-4: high recovery low energy desalination of brackish water by a new single stage method without any loss of brine energy, Desalin. Water Treat. 42 (2012) 262–268.
[18] Z. Wang, A. Deshmukh, Y. Du, M. Elimelech, Minimal and zero liquid discharge with reverse osmosis using low-salt-rejection membranes, Water Res. 170 (2020), 115317.
[19] A.A. Atia, N.Y. Yip, V. Fthenakis, Pathways for minimal and zero liquid discharge with enhanced reverse osmosis technologies: module-scale modeling and techno-economic assessment, Desalination 509 (2021), 115069.
[20] Y. Muhammad, W. Lee, Zero-liquid discharge (ZLD) technology for resource recovery from wastewater: a review, Sci. Total Environ. 681 (2019) 551–563.
[21] Y. Oren, E. Korngold, N. Daltrophe, R. Messalem, Y. Volkman, L. Aronov, M. Weismann, N. Bouriakov, P. Glueckstern, J. Gilron, Pilot studies on high recovery BWRO-EDR for near zero liquid discharge approach, Desalination 261 (2010) 321–330.
[22] R. Schwantes, K. Chavan, D. Winter, C. Felsmann, J. Pfafferott, Techno-economic comparison of membrane distillation and MVC in a zero liquid discharge application, Desalination 428 (2018) 50–68.
[23] C.D. Peters, N.P. Hankins, Osmotically assisted reverse osmosis (OARO): five approaches to dewatering saline brines using pressure-driven membrane processes, Desalination 458 (2019) 1–13.
[24] C.D. Peters, N.P. Hankins, The synergy between osmotically assisted reverse osmosis (OARO) and the use of thermo-responsive draw solutions for energy efficient, zero-liquid discharge desalination, Desalination 493 (2020), 114630.
[25] T.V. Bartholomew, L. Mey, J.T. Arena, N.S. Siefert, M.S. Mauter, Osmotically assisted reverse osmosis for high salinity brine treatment, Desalination 421 (2017) 3–11.
[26] A.T. Bouma, J.H. Lienhard, Split-feed counterflow reverse osmosis for brine concentration, Desalination 445 (2018) 280–291.
[27] K. Park, D.Y. Kim, D.R. Yang, Cost-based feasibility study and sensitivity analysis of a new draw solution assisted reverse osmosis (DSARO) process for seawater desalination, Desalination 422 (2017) 182–193.
[28] D.M. Davenport, A. Deshmukh, J.R. Werber, M. Elimelech, High-pressure reverse osmosis for energy-efficient hypersaline brine desalination: current status, design considerations, and research needs, Environ. Sci. Technol. Lett. 5 (2018) 467–475.
[29] X. Chen, N.Y. Yip, Unlocking high-salinity desalination with cascading osmotically mediated reverse osmosis: energy and operating pressure analysis, Environ. Sci. Technol. 52 (2018) 2242–2250.
[30] J. Martínez, E. León, F.M. Baena-Moreno, M. Rodríguez-Galán, F. Arroyo-Torralvo, L.F. Vilches, Techno-economic analysis of a membrane-hybrid process as a novel low-energy alternative for zero liquid discharge systems, Energy Convers. Manag. 211 (2020), 112783.
[31] J. Kim, J. Kim, J. Kim, S. Hong, Osmotically enhanced dewatering-reverse osmosis (OED-RO) hybrid system: implications for shale gas produced water treatment, J. Membr. Sci. 554 (2018) 282–290.
[32] N. Togo, K. Nakagawa, T. Shintani, T. Yoshioka, T. Takahashi, E. Kamio, H. Matsuyama, Osmotically assisted reverse osmosis utilizing hollow fiber membrane module for concentration process, Ind. Eng. Chem. Res. 58 (2019) 6721–6729.
[33] N.S. Siefert, J. Arena, M. Mauter, Dewatering of high salinity brines by osmotically assisted reverse osmosis (ASME 2017 power conference), in: NETL, 2017.
[34] T.H. Chong, S.-L. Loo, W.B. Krantz, Energy-efficient reverse osmosis desalination process, J. Membr. Sci. 473 (2015) 177–188.
[35] T.H. Chong, S.-L. Loo, A.G. Fane, W.B. Krantz, Energy-efficient reverse osmosis desalination: effect of retentate recycle and pump and energy recovery device efficiencies, Desalination 366 (2015) 15–31.
[36] S. Kürklü, S. Velioğlu, M.G. Ahunbay, S.B. Tantekin-Ersolmaz, W.B. Krantz, A novel energy-efficient concurrent desalination and boron removal (CDBR) process, Desalination 423 (2017) 79–94.
[37] M.G. Ahunbay, S.B. Tantekin-Ersolmaz, W.B. Krantz, Energy optimization of a multistage reverse osmosis process for seawater desalination, Desalination 429 (2018) 1–11.
[38] T.H. Chong, W.B. Krantz, Process economics and operating strategy for the energy-efficient reverse osmosis (EERO) process, Desalination 443 (2018) 70–84.
[39] K. Jeong, M. Park, T.H. Chong, Numerical model-based analysis of energy-efficient reverse osmosis (EERO) process: performance simulation and optimization, Desalination 453 (2019) 10–21.
[40] W.B. Krantz, T.H. Chong, Centrifugal reverse osmosis (CRO)– a novel energy-efficient membrane process for desalination near local thermodynamic equilibrium, J. Membr. Sci. 637 (2021), 119630.
[41] R.L. Stover, Industrial and brackish water treatment with closed circuit reverse osmosis, Desalin. Water Treat. 51 (2013) 1124–1130.
[42] S. Lin, M. Elimelech, Staged reverse osmosis operation: configurations, energy efficiency, and application potential, Desalination 366 (2015) 9–14.
[43] P.A. Davies, A solar-powered reverse osmosis system for high recovery of freshwater from saline groundwater, Desalination 271 (2011) 72–79.
[44] E. Hosseinipour, K. Park, L. Burlace, T. Naughton, P.A. Davies, A free-piston batch reverse osmosis (RO) system for brackish water desalination: experimental study and model validation, Desalination 527 (2022), 115524.
[45] M. Barello, D. Manca, R. Patel, I.M. Mujtaba, Operation and modeling of RO desalination process in batch mode, Comput. Chem. Eng. 83 (2015) 139–156.
[46] K. Park, L. Burlace, N. Dhakal, A. Mudgal, N.A. Stewart, P.A. Davies, Design, modelling and optimisation of a batch reverse osmosis (RO) desalination system using a free piston for brackish water treatment, Desalination 494 (2020), 114625.
[47] P.A. Davies, J. Wayman, C. Alatta, K. Nguyen, J. Orfi, A desalination system with efficiency approaching the theoretical limits, Desalin. Water Treat. 57 (2016) 23206–23216.
[48] S. Cordoba, A. Das, J. Leon, J.M. Garcia, D.M. Warsinger, Double-acting batch reverse osmosis configuration for best-in-class efficiency and low downtime, Desalination 506 (2021), 114959.
[49] T. Qiu, P.A. Davies, Comparison of configurations for high-recovery inland desalination systems, Water 4 (2012).
[50] Q.J. Wei, C.I. Tucker, P.J. Wu, A.M. Trueworthy, E.W. Tow, J.H. Lienhard, Impact of salt retention on true batch reverse osmosis energy consumption: experiments and model validation, Desalination 479 (2020), 114177.
[51] Z. Gal, A. Efraty, CCD series no. 18: record low energy in closed-circuit desalination of Ocean seawater with nanoH2O elements without ERD, Desalin. Water Treat. 57 (2016) 9180–9189.
[52] A. Efraty, J. Septon, Closed circuit desalination series no-5: high recovery, reduced fouling and low energy nitrate decontamination by a cost-effective BWRO-CCD method, Desalin. Water Treat. 49 (2012) 384–389.
[53] A. Efraty, Closed circuit desalination series no-3: high recovery low energy desalination of brackish water by a new two-mode consecutive sequential method, Desalin. Water Treat. 42 (2012) 256–261.
[54] N. Kahraman, Y.A. Cengel, B. Wood, Y. Cerci, Exergy analysis of a combined RO, NF, andEDR desalination plant, Desalination 171 (2005) 217–232.
[55] I.H. Aljundi, Second-law analysis of a reverse osmosis plant in Jordan, Desalination 239 (2009) 207–215.
[56] A.A. Alsarayreh, M.A. Al-Obaidi, A. Ruiz-García, R. Patel, I.M. Mujtaba, Thermodynamic limitations and exergy analysis of brackish water reverse osmosis desalination process, Membranes 12 (2022).
[57] Hyrec, www.hyrec.co, See report on, https://www.bluetechforum.com/wp-content/uploads/Hyrec-BlueTech-Forum-2018-Innovation-Showcase_HYREC_GM-version-2.pdf. (Accessed 25 April 2022). High recovery, membrane based, non thermal concentration technology to treat produced water, in.
[58] D. Cingolani, F. Fatone, N. Frison, M. Spinelli, A.L. Eusebi, Pilot-scale multi-stage reverse osmosis (DT-RO) for water recovery from landfill leachate, Waste Manag. 76 (2018) 566–574.
[59] I.H. Aljundi, Second-law analysis of a reverse osmosis plant in Jordan, Desalination 239 (2009) 207–215.
[60] T. Qiu, P.A. Davies, Longitudinal dispersion in spiral wound RO modules and its effect on the performance of batch mode RO operations, Desalination 288 (2012) 1–7.
[61] A. Haidari, S. Heijman, W. van der Meer, Visualization of hydraulic conditions inside the feed channel of reverse osmosis: a practical comparison of velocity between empty and spacer-filled channel, Water Res. 106 (2016) 232–241.
[62] C.P. Koutsou, S.G. Yiantsios, A.J. Karabelas, A numerical and experimental study of mass transfer in spacer-filled channels: effects of spacer geometrical characteristics and schmidt number, J. Membr. Sci. 326 (2009) 234–251.
[63] L. Wang, C. Violet, R.M. DuChanois, M. Elimelech, Derivation of the theoretical minimum energy of separation of desalination processes, J. Chem. Educ. 97 (2020) 4361–4369.
[64] B. Massey, Mechanics of Fluids, 4. th Edition, The English Language Book Society, 1980.
[65] J.H. Lienhard, G.P. Thiel, D.M. Warsinger, L.D. Banchik, Low Carbon Desalination: Status and Research, Development, and Demonstration Needs, Report of a Workshop Conducted at the Massachusetts Institute of Technology in Association With the Global Clean Water Desalination Alliance, 2016.
[66] M.H. Sharqawy, S.M. Zubair, Second law analysis of reverse osmosis desalination plants: an alternative design using pressure retarded osmosis, Energy 36 (2011) 6617–6626.
[67] A.A. Alsarayreh, M.A. Al-Obaidi, A. Ruiz-García, R. Patel, I.M. Mujtaba, Thermodynamic limitations and exergy analysis of brackish water reverse osmosis desalination process, Membranes 12 (2021) 11.
[68] H. Shimura, Development of an advanced reverse osmosis membrane based on detailed nanostructure analysis, Polym. J. 54 (2022) 767–773.
[69] D.M. Davenport, L. Wang, E. Shalusky, M. Elimelech, Design principles and challenges of bench-scale high-pressure reverse osmosis up to 150 bar, Desalination 517 (2021), 115237.